Application of a New MPIE Formulation to the Analysis of a Dielectric Resonator Embedded in a Multilayered Medium Coupled to a Microstrip Circuit

Jingyang Chen, *Member, IEEE*, Ahmed A. Kishk, *Fellow, IEEE*, and Allen W. Glisson, *Senior Member, IEEE*

***Abstract*—A new mixed-potential integral-equation (MPIE) formulation is developed for the analysis of electromagnetic problems due to conducting or dielectric objects of arbitrary shape embedded in a planarly stratified medium. In the new MPIE formulation, the dyadic kernel of the vector potential is kept in the simple form originally developed by Sommerfeld. The scalar potential, which is related to the vector potential via the Lorenz gauge, is then represented by a double dot product of a dyadic kernel with a dyadic charge density. An extra line integral term, which is well behaved and nonsingular, will appear when the object penetrates an interface. The numerical implementation of the double dot product is found to be trivial if one takes advantage of the well-established basis functions in which the unknown current density is expressed. The new MPIE formulation is employed in conjunction with the triangular patch model to treat the problem of a dielectric resonator (DR) excited by microstrip circuit. A matched-load simulation procedure has been used to extract the network S-parameters of a DR microstrip circuit. The diameters of the Q circles have been measured to determine the coupling coefficients and the Q factors of the DR excited by a microstrip circuit. The validity of the new MPIE formulation and the numerical procedure have been verified by comparing the obtained S-parameters with available measurement data.**

***Index Terms*—Boundary integral equations, dielectric antennas, dielectric bodies, dielectric resonators, electromagnetic coupling, Green's function, microstrip circuits, moment methods, nonhomogeneous media, numerical analysis.**

I. Introduction

MOST of the method of moments (MoM) analysis techniques available for microstrip structures are limited to planar geometries consisting of only horizontal current components. However, the development of a model for dielectric resonators (DRs) coupled to microstrip circuits requires an accurate analysis method that is valid for objects of arbitrary shape residing on or penetrating into a multilayered medium. The same problem arises even for simple structures such as coax-fed microstrip patches or microstrip circuits whose thicknesses cannot be neglected. The MoM procedure for microstrip circuits can be applied either in the spatial domain [1]–[5] or the spectral domain [6]–[9]. The spectral-domain analysis is more suitable and efficient for planar structures, while the spatial-domain analysis is more general in that it can be easily applied to objects of arbitrary shape. Michalski presented the mixed-potential integral-equation (MPIE) approach in [10]. However, it is usually more difficult to formulate an MPIE for an object of arbitrary shape in the presence of material layers, such as for a DR embedded in a microstrip circuit, due to the nonuniqueness of the potentials [11]. Later, Michalski and Zheng presented three formulations of the MPIE where the vector-potential dyadic kernel was modified so that only one scalar-potential kernel was required [12]. These formulations are amenable to increasing the capability of the well-established triangular patch MoM procedure, initially developed by Rao, Wilton, and Glisson (RWG) [13] for arbitrarily shaped geometries in free space. An advantage of the MPIE formulation is that vector and scalar potentials are employed, and they are expressed, respectively, in terms of the current and charge densities. This type of equation is often preferable to other forms of the integral equations because less singular kernels and more rapidly convergent spectral integrals are involved.

The MPIE has been widely adopted to solve the problems of microstrip planar circuits in the spatial domain [3], [4], [14]. Vandenbosch and Capelle proposed and applied another MPIE, which employs two scalar-potential kernels (one for a horizontal dipole and the other for a vertical dipole) to analyze microstrip circuits consisting of both horizontal and vertical current components, but not having both components at the same location, such as coax-fed rectangular patch antennas [15].

We observe, however, that due to its vector nature, the numerical implementation of the vector potential in a local coordinate system results in three integrals [15]; in a planarly stratified structure, all these three integrals must be performed over a dyadic kernel, which results in 15 scalar integrals if the dyadic kernel of the vector potential is kept in the simplest form originally developed by Sommerfeld, and these integrations remain the most time-consuming part of the solution process. The modification of the dyadic kernel of the vector potential in Michalski's formulations has the undesirable effect of

Manuscript received March 2, 1999. This work was supported in part by the Army Research Office under Grant DAAG55-98-0308 and in part by the National Science Foundation under Grant ECS-9809862 and under Grant ECS-9810448.

J. Chen was with the Department of Electrical Engineering, University of Mississippi, University, MS 38677 USA. He is now with the Algorithm Group, Uplink Product Department, Broadband Communication Sector, San Diego, CA 92121 USA.

A. A. Kishk and A. W. Glisson are with the Department of Electrical Engineering, University of Mississippi, University, MS 38677 USA.

Publisher Item Identifier S 0018-9480(01)01066-3.

introducing two new nonzero entries, which results in six more scalar integrals, and which impacts the already time-consuming process. Thus, our goal is to keep the dyadic kernel of the vector potential in the simplest form, yet keep the scalar potential in a form compatible with the original implementation (in terms of charge density).

Recently, Michalski and Mosig presented a new MPIE formulation where the scalar-potential Green's function K^{ϕ} pertaining to a horizontal dipole was used throughout; the "scalar potential" was expressed in terms of the scalar-potential kernel $\langle K^{\phi},\ \nabla' \cdot \mathbf{J} \rangle$ and a "correction factor" $\langle C^{\phi},\ J_z \rangle$, which avoids the undesirable effect of modification of the vector potential by not grouping the "correction factor" with the vector-potential term [16]. A similar work by Montgomery and Wilton can be found in [17] and [18], where the "correction factor" was intentionally left with the "scalar potential" so that the vector-potential dyadic Green's function remained unmodified, while the scalar potential was expressed in terms of both charge and current densities.

The objective of this paper is to extend the existing RWG MoM technique for free-space problems to multilayered media problems and, specifically, to model DR circuit configurations. First, two new MPIE formulations are developed systematically. As usual, the vector potential is represented by a dot product of a dyadic kernel with the vector current density. Consequently, the scalar potential, which is related to the vector potential via the Lorenz gauge, cannot be described with a single scalar kernel. This is due to the well-known fact that the scalar potentials of a single point charge associated with a horizontal and vertical dipole in a multilayered medium are, in general, not identical [10]. In other words, the scalar potential depends not only on the value, but also the flow direction of the charge. A static point charge, on the other hand, produces a unique potential. This can be verified by the fact that the static portions extracted from the scalar potentials due to both horizontal and vertical dipoles are equal to each other. A systematic solution for this anisotropic problem is to employ a dyadic kernel to represent the scalar potentials [19], where a dyadic charge density is introduced in the expressions. In this paper, two new formulations of the MPIE are proposed in which the scalar potential is represented by a double-dot product of a dyadic kernel with the dyadic charge distribution. One of the formulations has been found suitable for penetrating geometries and is easily implemented in a MoM procedure. In this formulation, the dyadic kernel of the vector potential is kept in the simple form originally developed by Sommerfeld [20]. The tradeoff is that the scalar potential has to be expressed with a dyadic kernel. An extra line integral term, which is well behaved and nonsingular, will appear when the object penetrates an interface. The numerical implementation of the double-dot product is found to be trivial if one takes advantage of the well-established RWG basis functions in which the unknown current density is expressed. One of these two formulations has recently been adopted and applied to analyze the circumferential variation of the longitudinal current distributions on a thin-wire antenna protruding through an interface between two layered medium [21].

The first part of this paper is dedicated to the description of the two MPIE formulations. The general geometry to be considered is described in Section II and a system of MPIE integral equations is presented for the problem under consideration. In Section III, the dyadic Green's functions of the scalar potentials involved in the integral equations are deduced from a general form for the vector-potential dyadic Green's functions. The derivation of the general form for the vector-potential dyadic Green's function is outlined in the Appendix. The cylindrical vector wave functions used as the modal functions in the derivation are described in [22, App. C], where some of the relations of the wave functions, which have not been listed in literature yet, are also presented. The properties of the scalar-potential dyadic Green's functions are discussed in Section IV.

The numerical implementation with the MoM is presented in Section II of this paper to analyze the problem of a DR excited by microstrip circuit. In conjunction with the widespread development of wireless information networks such as cellular, personal communication services (PCSs), satellite communication systems, mobile computing, and other new systems and services, monolithic microwave integrated circuits (MMICs) have advanced significantly in the past few years. The primary motivation for developing MMICs in wireless communications such as PCSs is to achieve higher quality, longer battery lifetime, lower cost, and lighter terminals [23]. DRs with high-permittivity and low-temperature coefficients are smaller than waveguide or coaxial resonators, are easily fabricated, and are compatible with MMIC implementation [24], [25]. Using DRs, instead of metal cavities, in a multilayered medium coupled to a microstrip line or a slot aperture, eliminates the need for microstrip-to-cavity adapters and provides great flexibility to realize complicated bilateral and multilayered printed circuits, thus allowing very compact high-density circuit integration.

With the advent of the high dielectric-constant and low-temperature coefficient ceramic materials, the applications of the DR in the design of passive and active microwave circuits [26], [27] have spread toward low frequencies for mobile communications such as PCSs at 1.8–2 GHz. An experimental study of a DR, of relative dielectric constant 80 and of resonant frequency about 1.7 GHz, coupled to a microstrip line can be found in [28]. The MoM has been used to calculate the characteristics of an isolated DR that is of the body-of-revolution type [29], [30]. This model includes both dielectric and radiation losses. Numerical analysis of in-circuit parameters of a DR is more challenging. Recently, a study of the DR antennas excited by a coaxial probe or slot aperture has been conducted both in theory and measurement at the University of Mississippi, University [31]–[33], where the theoretical investigations have considered mainly structures consisting of body-of-revolution DRs combined with wires or slots.

The new MPIE formulation developed in this paper is used here in conjunction with the triangular patch model, originally developed for arbitrarily shaped objects in free space, to model the problem of a DR excited by microstrip circuit. The numerical procedure has been modified to handle the potential dyadic kernels and the dyadic charge density, as described in Section VI. Section VII briefly describes a matched-load simulation procedure that has been used to extract the network S-parameters of a DR microstrip circuit. The diameters of the

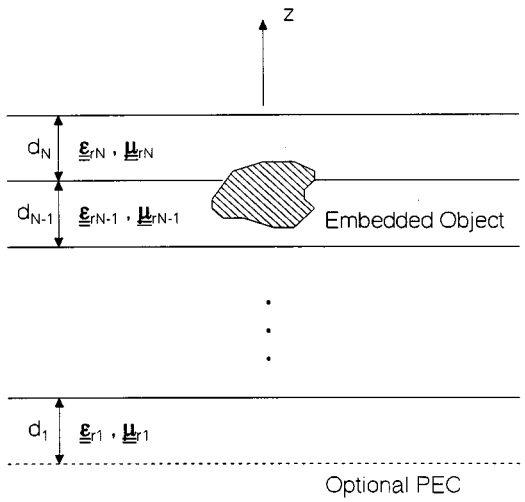

Fig. 1. General geometry under consideration.

Q circles have been also measured to determine the coupling coefficients and the Q factors of the DR excited by a microstrip circuit. The validity of the new MPIE formulation and the numerical procedure have been verified by comparing the obtained S-parameters with available measurement data in Section VIII, and a summary is provided in Section IX.

II. Preliminaries

This section contains the statement of the general geometry to be considered. A preliminary description of the new MPIE formulations is also presented for the problem under consideration. The detailed mathematical expressions and the properties of the potential dyadic Green's functions involved in the integral equation are presented in the two subsequent sections.

A. General Geometry Under Consideration

The cross-sectional view of the structure under consideration is shown in Fig. 1. The medium consists of N planar dielectric layers, with the layer interfaces parallel to the x–y-plane. The relative permittivity and permeability of the layered medium are given by the tensor

$$\overline{\boldsymbol{\alpha}}'(z) = \overline{\mathbf{I}}_t \alpha_t'(z) + \hat{\mathbf{z}}\hat{\mathbf{z}}\alpha_z'(z) \tag{1}$$

where the subscript t denotes components in the plane perpendicular to $\hat{\mathbf{z}}$, and

$$\overline{\mathbf{I}}_\mathbf{t} = \begin{bmatrix} 1 & 0 \\ 0 & 1 \end{bmatrix} \quad \alpha_t'(z) = \begin{Bmatrix} \epsilon_t'(z) \\ \mu_t'(z) \end{Bmatrix} \quad \alpha_z'(z) = \begin{Bmatrix} \epsilon_z'(z) \\ \mu_z'(z) \end{Bmatrix}.$$

It is also convenient to define an anisotropy ratio $v_\alpha = \alpha_z'/\alpha_t'$ for the layer. Each layer of the medium, say, the nth layer, is assumed homogeneous and is characterized by α_{tn}' and α_{zn}'.

The object shown in Fig. 1 is embedded in the multilayered structure and may consist of conducting and/or dielectric materials. The equivalence principle is employed to replace the object with unknown equivalent surface currents. By enforcing the boundary conditions on the surface of the object, a system of integral equations for the unknown currents can be established as follows:

$$\mathbf{E}_e^{\text{inc}}|_{\tan} = -\mathbf{E}_e^s|_{\tan}, \qquad \text{on } S_c \tag{2a}$$

$$\mathbf{E}_e^{\text{inc}}|_{\tan} + \mathbf{E}_e^s|_{\tan} = \mathbf{E}_d^s|_{\tan}, \qquad \text{on } S_d \tag{2b}$$

$$\mathbf{H}_e^{\text{inc}}|_{\tan} + \mathbf{H}_e^s|_{\tan} = \mathbf{H}_d^s|_{\tan}, \qquad \text{on } S_d. \tag{2c}$$

In (2), subscripts e and d denote the exterior and interior regions, respectively, and superscripts inc and s denote the incident field and the scattered field due to the equivalent currents. S_c and S_d represent the conducting and dielectric surfaces, respectively.

B. MPIE Formulation

The fields in (2) can be written as the mixed-potential forms [34]

$$\mathbf{E}^s = -j\omega\mathbf{A} - \nabla\phi^e - \frac{1}{\epsilon}\nabla\times\mathbf{F} \tag{3a}$$

$$\mathbf{H}^s = -j\omega\mathbf{F} - \nabla\phi^m + \frac{1}{\mu}\nabla\times\mathbf{A} \tag{3b}$$

where $\mathbf{A}$ is the magnetic vector potential due to the electric current density $\mathbf{J}$, and is given as

$$\mathbf{A} = \int\int_s \overline{\mathbf{G}}^A \cdot \mathbf{J}(\mathbf{r}')\, ds'. \tag{4}$$

The electric scalar potential is related to the vector potential by the Lorenz gauge to obtain

$$\phi^e = \frac{j\omega}{k_0^2\mu_t'\epsilon_t'} \int\int_s \nabla\cdot\overline{\mathbf{G}}^A \cdot \mathbf{J}(\mathbf{r}')\, ds'. \tag{5}$$

To deduce the scalar-potential Green's function, one needs to transform the divergence operator to act on the current density. To do so, it is postulated that

$$\frac{j\omega}{k_0^2\mu_t'\epsilon_t'}\nabla\cdot\overline{\mathbf{G}}^A(\mathbf{r},\mathbf{r}') = \nabla'\cdot\overline{\mathbf{G}}^e(\mathbf{r},\mathbf{r}'). \tag{6}$$

One can always find a dyadic kernel $\overline{\mathbf{G}}^e$ that satisfies (6) although it may not be unique. Equation (6) is a vector equation, which renders three scalar equations, but there are nine entries in $\overline{\mathbf{G}}^e$ to determine. It will always be possible to choose some of the entries as "correction factors" that make (6) hold. Of course, one would like to have most of the entries to be zero. With a dyadic kernel on the right-hand side, our goal can be achieved. If instead a scalar kernel is used, as in [12, eq. (12)], in general, one would not be able to find a scalar kernel that satisfies [12, eq. (12)] without modifying the vector-potential kernel because there is only one function to determine and it must satisfy all three scalar equations that are rendered from a vector equation. However, if the three scalar equations are identical or similar (as in free space), the scalar kernel exists. Unfortunately, this is not the case for layered medium where a "correction factor" $\mathbf{P}$, as in [12, eq. (13)] has to be introduced. However, by using a dyadic kernel and the dyadic identities [35]

$$\nabla\cdot(\overline{\mathbf{A}}\cdot\mathbf{B}) = \nabla\cdot\overline{\mathbf{A}}\cdot\mathbf{B} + \overline{\mathbf{A}} : \nabla\mathbf{B}$$

and

$$\int\int_s \nabla\cdot(\overline{\mathbf{A}}\cdot\mathbf{B})\, ds = \int_{\partial s} \overline{\mathbf{A}}\cdot\mathbf{B}\cdot\hat{\mathbf{u}}\, dl \tag{7}$$

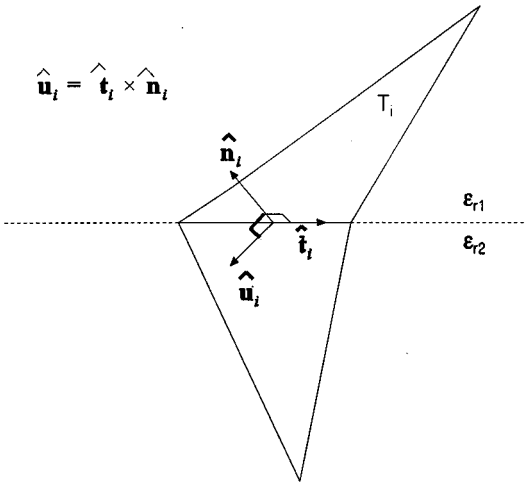

Fig. 2. Definition of $\hat{\mathbf{u}}$ in the upper medium for a triangle pair penetrating an interface.

the equation for the scalar potential can be written as

$$\phi^e = \int_{\partial s} \left[\overline{\mathbf{G}}^e(\mathbf{r}, \mathbf{r}') \cdot \mathbf{J}(\mathbf{r}')\right] \cdot \hat{\mathbf{u}}\, dl' + \int\int_s \overline{\mathbf{G}}^e(\mathbf{r}, \mathbf{r}') : \nabla' \mathbf{J}(\mathbf{r}')\, ds' \quad (8)$$

where ∂s is the line formed by the intersection of the body surface and the interface with the layer surface, the unit vector $\hat{\mathbf{u}}$ lies in the plane tangential to the surface of the object and is perpendicular to ∂s, as shown in Fig. 2, and $\hat{\mathbf{n}}_i$ is the unit vector normal to the surface of the triangle T_i. It should be pointed out that the line integral will disappear if the object is confined in a single layer.

It is proved in the following section that the scalar-potential dyadic Green's function has the following general form:

$$\overline{\mathbf{G}}^e(\mathbf{r}, \mathbf{r}') = \begin{bmatrix} G_h^e & 0 & 0 \\ 0 & G_h^e & 0 \\ 0 & 0 & G_v^e \end{bmatrix} \quad (9)$$

where G_h^e is related to the charge density associated with the horizontal current component, while G_v^e is related to the charge density associated with vertical current component. For the traditional formulation, G_h^e is a continuous function as both the source and field points cross the interface, while G_v^e is continuous as the field point crosses the interface, but is discontinuous as the source point crosses the interface. Using these features, the line integral appearing in (8) can be further simplified upon observing that

$$\begin{aligned} \overline{\mathbf{G}}^e \cdot \mathbf{J} &= G_h^e J_x \hat{\mathbf{x}} + G_h^e J_y \hat{\mathbf{y}} + G_v^e J_z \hat{\mathbf{z}} \\ &= G_h^e \mathbf{J} + (G_v^e - G_h^e) J_z \hat{\mathbf{z}}. \end{aligned} \quad (10)$$

Since G_h^e is a continuous function, the first term in (10) will cancel out when the line integral is implemented on the penetrating edge just above and below the interface. Thus, (8) becomes

$$\phi^e = \int_{\partial s} \left[(G_v^e - G_h^e) J_z \hat{\mathbf{z}}\right] \cdot \hat{\mathbf{u}}\, dl' + \int\int_s \overline{\mathbf{G}}^e(\mathbf{r}, \mathbf{r}') : \nabla' \mathbf{J}(\mathbf{r}')\, ds'. \quad (11)$$

Since G_v^e and G_h^e have the same singular behavior, the line integral in (11) is well behaved and nonsingular.

Although our objective is to derive the potential dyadic Green's functions, it is more convenient to derive the field counterparts initially because the fields are unique while the potentials are not. Also, the expressions of the boundary conditions on the interfaces between two layers are more concise in terms of fields than in terms of potentials. In this paper, the cylindrical vector wave functions are chosen as the modal functions for a planarly stratified medium, and the modal function expansion procedure in [36] is then employed to derive the field dyadic Green's functions. The potential dyadic Green's functions are then deduced from the field counterparts. To conserve space, a general form for the vector dyadic Green's function is listed in the Appendix, where only the outline of the derivation is given. The scalar-potential dyadic Green's function will be derived, in the following section, from the general expression for the vector-potential dyadic Green's function.

To complete the description of the MPIE formulations, it should be mentioned that similar formulations and conclusions can be obtained for the electric vector and magnetic scalar potentials.

III. Scalar-Potential Dyadic Green's Functions in a Multilayered Uniaxial Medium

In this section, the scalar-potential dyadic Green's functions in a multilayered uniaxial medium are deduced from the vector-potential counterparts using the Lorenz gauge. The nonuniqueness and the properties of the potential Green's functions are discussed in the following section. The derivation of the field dyadic Green's functions in a planarly stratified medium has been well documented [36], [37]. In contrast, studies of potential (especially scalar potential) Green's functions due to an arbitrary source in a stratified medium have only been presented in academic journals [12], [19]. These studies have attracted attention since the 1980's due to the development of MPIE numerical procedures. The traditional way to derive potential Green's functions due to an arbitrary source starts by presuming an expression—either the traditional or alternative form [10]. Here, the derivation begins with the general expression for the vector potential in a uniaxial medium so that the vector potential due to an arbitrary source in a stratified uniaxial medium can be derived naturally without any presumptions. Unfortunately, the scalar potential, which is related to the vector potential by the Lorenz gauge, contains a simple pole at $k_\rho = 0$ in the spectral domain. This singularity has to be subtracted, otherwise problems arise in the numerical computations. Two formulations of vector and scalar potentials are presented here, which result from two different ways of subtracting the singularity. One of the formulations is subsequently implemented.

A. General Expressions of Scalar Potentials

In a layered uniaxial medium, the scalar potentials due to a single point charge associated with the horizontal and vertical dipoles are, in general, different [10], and one cannot calculate the scalar potentials due to an arbitrarily oriented dipole via an

integral with a single scalar kernel K^{ϕ}. Michalski and Zheng [12] choose K^{ϕ} to be the scalar potential of either the horizontal or vertical dipole, and then use a correction function $\nabla\mathbf{P}$ in the vector potential to account for the other part of the scalar potential.

In this section, the scalar potential due to an arbitrarily oriented dipole is formulated in a dyadic form. The scalar potential is related to the vector potential by the Lorenz gauge, as expressed in (5). Since the divergence operator would make the kernel more singular, we attempt to transfer the operator ∇ to act on the current density, so that the scalar potential can be expressed in terms of the charge density. From [22, eqs. (A-8a) and (C-7a)], one can obtain

$$\begin{aligned}\nabla\cdot\overline{\mathbf{G}}^{A}(\mathbf{r},\mathbf{r}') &= \nabla_t\overline{\mathbf{G}}^{A}(\mathbf{r},\mathbf{r}')+\frac{\partial}{\partial z}\left(\hat{\mathbf{z}}\cdot\overline{\mathbf{G}}^{A}(\mathbf{r},\mathbf{r}')\right)\\ &= \frac{\partial G^{A}_{zt}}{\partial z}\,\hat{\mathbf{t}}+\frac{\partial G^{A}_{zz}}{\partial z}\,\hat{\mathbf{z}}. \end{aligned}\tag{12}$$

In order to transform the divergence operator to the current density, we attempt to find a dyadic ,$\overline{\mathbf{G}}^{e}$, as defined in (6). In view of (6) and (12), $\overline{\mathbf{G}}^{e}$ can be written as

$$\overline{\mathbf{G}}^{e}=\mathbf{I}_t k^{e}_{h1}+\hat{\mathbf{z}}\hat{\mathbf{z}}k^{e}_{v}\tag{13}$$

where k^{e}_{h1} denotes the scalar potential of a single point charge associated with a horizontal electric dipole and k^{e}_{v} denotes the scalar potential of a single point charge associated with a vertical electric dipole. Substitution of (12) and (13) into (6) yields

$$\frac{j\omega}{k_0^2\mu'_{t\tau}\epsilon'_{t\tau}}\,\frac{\partial G^{A}_{zt}}{\partial z}\,\hat{\mathbf{t}}=-\nabla'_t k^{e}_{h1}\tag{14a}$$

$$\frac{j\omega}{k_0^2\mu'_{t\tau}\epsilon'_{t\tau}}\,\frac{\partial G^{A}_{zz}}{\partial z}=-\frac{\partial}{\partial z'}\,k^{e}_{v}.\tag{14b}$$

Using (14) with (A-8a), (A-5), and [22, eq. (C-7)], we find that k^{e}_{h1} and k^{e}_{v} may be written as

$$\begin{aligned}k^{e}_{h1} &= -\int_0^{\infty}\frac{1}{k_\rho^5}\sum_n\frac{k^{e}_{z\tau}k^{e}_{z\zeta}}{(1+\delta_0)\pi}\\ &\quad\cdot Z^{e}_{\tau\zeta}(z,z')n_{zn}(\rho)n^{*}_{zn}(\rho')\,dk_\rho \end{aligned}\tag{15a}$$

$$\begin{aligned}k^{e}_{v} &= -\int_0^{\infty}\frac{dk_\rho}{v_{\epsilon\zeta}k^{e}_{z\zeta}k_\rho^3}\sum_n\frac{k^{e}_{z\tau}}{(1+\delta_0)\pi}\\ &\quad\cdot Z^{e}_{\tau\zeta}(z,z')n_{zn}(\rho)n^{*}_{zn}(\rho')\,dk_\rho \end{aligned}\tag{15b}$$

where $v_{\epsilon\zeta}$ is the anisotropy ratio for the permittivity in the ζth layer and other parameters are defined in the Appendix.

A close examination of (15a) reveals that k^{e}_{h1} has a pole at $k_\rho=0$. The various ways to subtract the pole will lead to following formulations.

B. Formulation A

In order to subtract the pole of k^{e}_{h1} at $k_\rho=0$, one can assume

$$k^{e}_{h}=k^{e}_{h1}-k^{e}_{h2}\tag{16}$$

where

$$\begin{aligned}k^{e}_{h2} &= -\int_0^{\infty}\frac{1}{k_\rho^3}\sum_n\frac{1}{(1+\delta_0)\pi}\,\frac{k^{h}_{z\tau}k^{h}_{z\zeta}}{k_\rho^2}\\ &\quad\cdot Z^{h}_{\tau\zeta}(z,z')n_{zn}(\rho,k^{h}_{z\tau})n^{*}_{zn}(\rho',k^{h}_{z\zeta})\,dk_\rho. \end{aligned}\tag{17}$$

From (3)–(5), (12), and (14), we have

$$-\overline{\mathbf{G}}^{e}=j\omega\overline{\mathbf{G}}^{A}+\nabla\nabla'_t k^{e}_{h1}+\nabla\frac{\partial}{\partial z'}\,k^{e}_{v}\hat{z}=\overline{\mathbf{K}}^{A}+\nabla\nabla'\cdot\overline{\mathbf{G}}^{e}\tag{18}$$

where $\overline{\mathbf{G}}^{e}$ is the $\mathbf{E}$-field dyadic Green's function due to the electric current source and

$$\overline{\boldsymbol{K}}^{A}=j\omega\overline{\boldsymbol{G}}^{A}+\nabla\nabla'_t k^{e}_{h2}\tag{19a}$$

$$\overline{\boldsymbol{G}}^{e}=\boldsymbol{I}_t k^{e}_{h}+\hat{\boldsymbol{z}}\hat{\boldsymbol{z}}k^{e}_{v}.\tag{19b}$$

Substitution of (A-8a) and (17) into (19) yields

$$\begin{aligned}\mathbf{K}^{A} &= \int_0^{\infty}\frac{1}{k_\rho}\sum_n\frac{1}{(1+\delta_0)\pi}\,Z^{h}_{\tau\zeta}(z,z')\\ &\quad\cdot\left[\mathbf{m}_{tn}(\rho)\mathbf{m}^{*}_{tn}(\rho')+\mathbf{n}_{tn}(\rho)\mathbf{n}^{*}_{tn}(\rho')\right]dk_\rho\\ &\quad-\int_0^{\infty}\frac{1}{k_\rho^3}\sum_n\frac{k_0\eta_0}{(1+\delta_0)\pi}\,\mu'_{t\tau}\\ &\quad\cdot\left[k^{e}_{z\tau}T^{e}_{i\tau\zeta}(z,z')\mathbf{n}_{zn}(\rho)-k^{h}_{z\tau}T^{h}_{i\tau\zeta}(z,z')\mathbf{n}_{zn}(\rho',k^{h}_{z\tau})\right]\\ &\quad\cdot\mathbf{n}^{*}_{tn}(\rho')\,dk_\rho\\ &\quad+\int_0^{\infty}\frac{1}{k_\rho^3}\sum_n\frac{k_0\mu'_{t\tau}\epsilon'_{z\tau}}{(1+\delta_0)\pi}\,\frac{z^{e}_{\tau}z^{e}_{\zeta}}{v_{e\tau}v_{e\zeta}}\\ &\quad\cdot Y^{e}_{\tau\zeta}(z,z')\mathbf{n}_{zn}(\rho)\mathbf{n}^{*}_{zn}(\rho')\,dk_\rho \end{aligned}\tag{20a}$$

$$\begin{aligned}k^{e}_{h} &= \int_0^{\infty}\frac{1}{k_\rho^3}\sum_n\frac{1}{(1+\delta_0)\pi}\\ &\quad\cdot\left[\frac{k^{e}_{z\tau}k^{e}_{z\zeta}}{k_\rho^2}\,Z^{e}_{\tau\zeta}(z,z')n_{zn}(\rho)n^{*}_{zn}(\rho')\right.\\ &\quad\left.-\frac{k^{h}_{z\tau}k^{h}_{z\zeta}}{k_\rho^2}\,Z^{h}_{\tau\zeta}(z,z')n_{zn}(\rho,k^{h}_{z\tau})n^{*}_{zn}(\rho',k^{h}_{z\zeta})\right]dk_\rho \end{aligned}\tag{20b}$$

$$\begin{aligned}k^{e}_{\nu} &= -\int_0^{\infty}\frac{1}{k_\rho^3}\sum_n\frac{1}{(1+\delta_0)\pi}\,\frac{1}{v_{e\zeta}}\,\frac{k^{e}_{z\tau}}{k^{e}_{z\zeta}}\\ &\quad\cdot Z_{\tau\zeta}(z,z')n_{zn}(\rho)n^{*}_{zn}(\rho')\,dk_\rho. \end{aligned}\tag{20c}$$

By duality, we have

$$-\overline{\mathbf{G}}^{H}=\overline{\mathbf{K}}^{F}+\nabla\nabla'\cdot\overline{\mathbf{G}}^{m}\tag{21}$$

where $\overline{\mathbf{G}}^{H}$ is the $\mathbf{H}$-field dyadic Green's function due to the magnetic current source and

$$\overline{\mathbf{G}}^{m}=\mathbf{I}_t k^{m}_{h}+\hat{\mathbf{z}}\hat{\mathbf{z}}k^{m}_{v}.\tag{22}$$

The expressions for $\overline{\mathbf{K}}^{F}$, k^{m}_{h}, and k^{m}_{v} are similar to those for $\overline{\mathbf{K}}^{A}$, k^{e}_{h}, and k^{e}_{v} given in (20), but have been omitted for brevity. The full expressions can be found in [22].

C. Formulation B

An alternate way to subtract the pole of k_{h1}^e at $k_\rho = 0$ is to assume k_{h2}^e to be given by

$$k_{h2}^e = \int_0^\infty \frac{1}{k_\rho^3} \sum_n \frac{k_0^2}{(1+\delta_0)\pi} \frac{\mu'_{t\tau}\epsilon'_{t\tau}k_{z\zeta}^e}{k_\rho^2 k_{z\tau}^e} \cdot Z_{\tau\zeta}^e(z, z') n_{zn}(\rho) n_{zn}^*(\rho')\, dk_\rho. \quad (23)$$

Substitution of (A-8a) and (23) into (19) yields

$$\begin{aligned}\overline{\mathbf{K}}^A = &\int_0^\infty \frac{1}{k_\rho} \sum_n \frac{1}{(1+\delta_0)\pi} Z_{\tau\zeta}^h(z, z') \mathbf{m}_{tn}(\rho) \mathbf{m}_{tn}^*(\rho')\, dk_\rho \\ &+ \int_0^\infty \frac{1}{k_\rho} \sum_n \frac{1}{(1+\delta_0)\pi} \frac{k_0^2 \mu'_{t\tau}\epsilon'_{t\tau}}{(k_{z\tau}^e)^2} \\ &\cdot Z_{\tau\zeta}^e(z, z') \mathbf{n}_{tn}(\rho) \mathbf{n}_{tn}^*(\rho')\, dk_\rho \\ &+ \int_0^\infty \frac{1}{k_\rho} \sum_n \frac{1}{(1+\delta_0)\pi} \frac{k_0^2 \mu'_{t\tau}\epsilon'_{z\tau}}{k_\rho^2} \frac{z_\tau^e z_\zeta^e}{v_{\epsilon\tau} v_{\epsilon\zeta}} \\ &\cdot Y_{\tau\zeta}^e(z, z') \mathbf{n}_{zn}(\rho) \mathbf{n}_{zn}^*(\rho')\, dk_\rho \quad (24a)\end{aligned}$$

$$\begin{aligned}k_h^e = &\int_0^\infty \frac{1}{k_\rho^3} \sum_n \frac{1}{(1+\delta_0)\pi} \frac{k_{z\zeta}^e}{v_{\epsilon\tau} k_{z\tau}^e} \\ &\cdot Z_{\tau\zeta}^e(z, z') n_{zn}(\rho) n_{zn}(\rho) n_{zn}^*(\rho')\, dk_\rho. \quad (24b)\end{aligned}$$

The expressions for $\overline{\mathbf{K}}^F$ and k_h^m can again be obtained from duality and are provided in [22]. The scalar potentials k_v^e and k_v^m of a single charge associated with vertical dipoles are in the same forms as in Formulation A.

IV. Discussion

Two formulations have been derived systematically in the previous section. It is worth noting that the vector-potential dyadic Green's functions in Formulations A and B are, respectively, in the traditional and alternative forms [37], and here, we simply derive them in a different way (from a general expression). In order to keep the vector potential in these two simplest forms, a dyadic charge density is introduced, and the scalar potential is represented by a double-dot product of a dyadic kernel $\overline{\mathbf{G}}^e$ or $\overline{\mathbf{G}}^m$ with the dyadic charge density. In Formulation A, $\overline{\mathbf{G}}^e$ and $\overline{\mathbf{G}}^m$ involve all of the four Green's functions of a multisectional transmission line, and k_h^e and k_h^m are continuous as both source and field points cross the interfaces, while k_v^e and k_v^m are continuous as the field point crosses the interfaces, but discontinuous as the source point crosses the interfaces. In Formulation B, $\overline{\mathbf{G}}^e$ and $\overline{\mathbf{G}}^m$ involve only two of the four Green's functions of the multisectional transmission line, and k_h^e and k_h^m are continuous as the source point crosses the interfaces, but discontinuous as the field point crosses the interfaces, while k_v^e and k_v^m are continuous as the field point crosses the interfaces, but discontinuous as the source point crosses the interfaces. When the embedded objects are confined in a single layer, k_h^e and k_h^m are, respectively, equal to k_v^e and k_v^m in Formulation B. In general, the dyadic Green's functions of the scalar potentials involved in (8) are discontinuous as the source point crosses the interfaces in Formulation A, however they are discontinuous as either the source or field point crosses an interface in Formulation B. In view of (3), during the testing procedure, one may prefer to transfer the gradient operators to act on the testing functions. If Formulation A is employed, no additional contour integrals appear during the testing procedure.

It is worth noting that the double-dot product in (11) will reduce to a scalar product if G_v^e and G_h^e are the same. Actually, by properly choosing k_{h2}^e in (16) or rearranging (18), one can derive a scalar Green's function for ϕ^e. Unfortunately, it will result in more nonzero entries in the vector-potential dyadic Green's function.

The numerical implementation of Formulation A, in conjunction with the triangular patch model, is given in the second part of this paper. For the sake of efficiency, the implementation of the vector potentials is conducted in a local coordinate system [13], which results in three integrals over the source triangle. The three integral kernels are, respectively, $\xi_1\overline{\mathbf{K}}^A$, $\xi_2\overline{\mathbf{K}}^A$, and $\overline{\mathbf{K}}^A$. In Michalski's Formulation C, $\overline{\mathbf{K}}^A$ contains seven nonzero entries, which results in a total of 21 scalar integrals for the vector potentials, plus one for the scalar potentials, and they all are singular. With Formulation A presented in this paper, $\overline{\mathbf{K}}^A$ contains only five nonzero entries, which results in a total of 15 scalar integrals for the vector potentials. The tradeoff, as will be stated in the second part of this paper, is that an extra scalar integral, which does not occur for objects in free space, appears for the scalar potentials. Furthermore, a line integral along the penetrating edges will occur when the object penetrates the interfaces. However, these two integrals are nonsingular and well behaved. As can be seen from the above analysis, Formulation A presented in this paper is more efficient, but one may need to add a code segment in the preprocessor to keep track of the penetrating edges, and one may also need to add a subroutine to carry out the line integral.

V. Applications

A. DR Coupled to a Microstrip Line

One specific configuration of interest in this paper is that of a DR coupled to a microstrip line. A DR in a multilayered medium coupled to a microstrip line can be used whenever a resonator is needed in a microstrip circuit. In theory, the resonant frequency can be determined by the resonant mode, dimensions, and permittivity of the DR along with the circuit environment, and the coupling coefficient can be adjusted by varying the distance from the DR to the edge of the microstrip line. In practice, however, the exact in-circuit resonant frequency cannot be predicted precisely due to the thermal expansion and the dimension tolerances of both the resonator and microstrip line. A simple, but effective tuning mechanism was introduced by Buer and El-Sharawy [38], where a nonresonant section of a microstrip line was employed to adjust the resonant frequency by offsetting the resonator with respect to the center of the tuning line. The position of the DR with respect to the microstrip feed line is also crucial in order to excite the desired mode. Thorough studies of different modes of DRs have been conducted in the Department of Electrical Engineering, University of Mississippi [24]. The studies have been continuing in both experimental and theoretical aspects in order to attain sufficient knowledge about

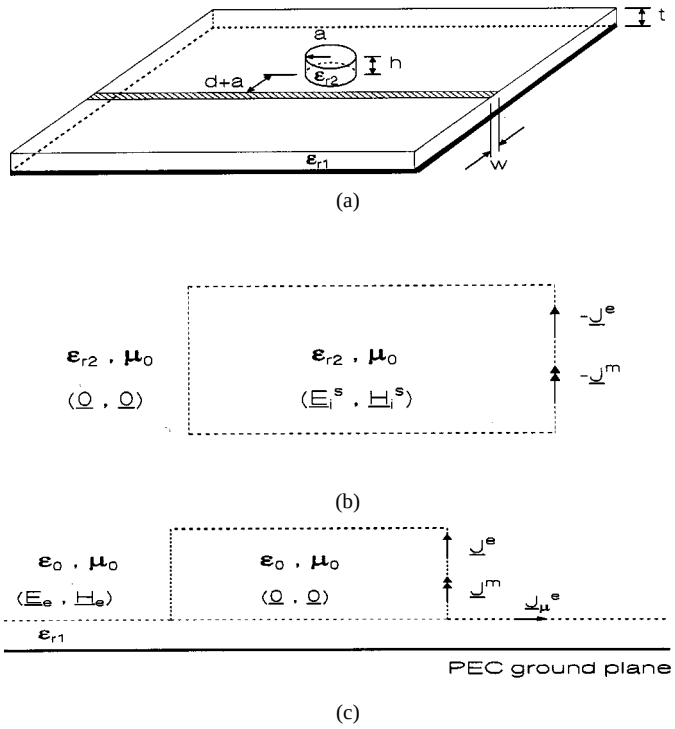

Fig. 3. Geometry and mathematical models of a DR coupled to a microstrip line. (a) Geometry of a DR coupled to a microstrip line. (b) Equivalent problem for the interior region. (c) Equivalent problem for the exterior region.

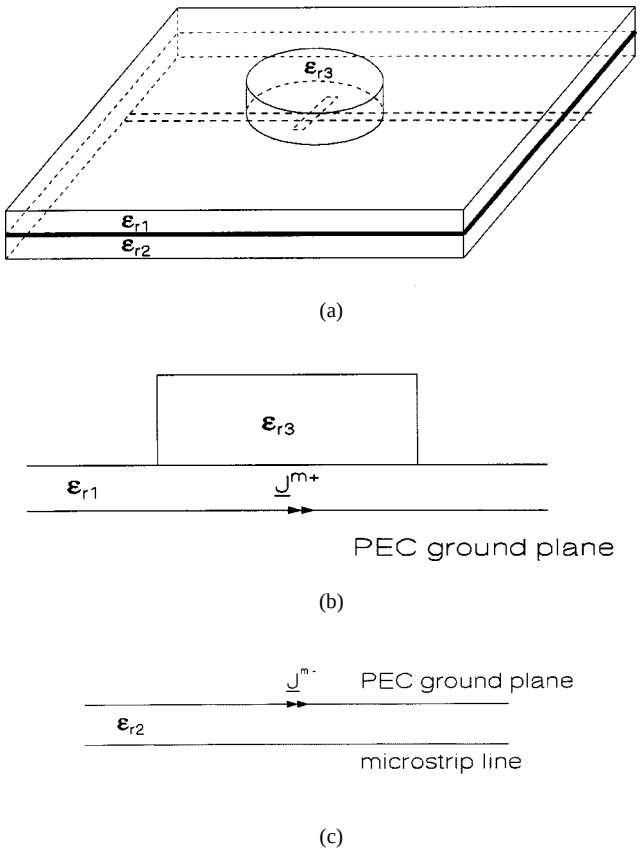

Fig. 4. Mathematical models of a DR coupled a slot aperture. (a) Geometry of a DR coupled to a slot aperture. (b) Equivalent problem for the upper half-space. (c) Equivalent problem for the lower half-space.

the frequency response of a DR coupled to microstrip circuit in a variety of circumstances.

In practice, the two lowest modes $\mathrm{TE}_{01\delta}$ and $\mathrm{HEM}_{11\delta}$ have been used primarily [24]. The former has a high unloaded quality factor and remains the primary choice for resonator use in a microstrip circuit, while the latter is a strong radiation mode and has been selected as an antenna [31]. The configuration for coupling of the $\mathrm{TE}_{01\delta}$ mode to a microstrip line is shown in Fig. 3(a). In accordance with the surface equivalence principle [34], the original problem can be divided into two problems. Fig. 3(b) illustrates the equivalent problem for the region interior to the surface of the DR, where the homogeneous space Green's function is employed through potential functions to represent the field quantities. Fig. 3(c) illustrates the equivalent problem for the region exterior to the surface of the DR, where the multilayered medium Green's functions are used in terms of appropriate potential functions to express the electric and magnetic fields. By enforcing the boundary conditions that the tangential components of the electric field must vanish on the conductor surface, and that the tangential components of both the electric and magnetic fields must be continuous across the dielectric surface, a system of integral equations can be established to determine the unknown equivalent currents $\mathbf{J}^e$ and $\mathbf{J}^m$. This system of equations can be found in (2).

B. DR Coupled to a Slot Aperture

Another specific configuration of interest in this paper is that of a DR coupled to a slot aperture. Fig. 4(a) illustrates the geometry of a DR coupled to a slot aperture. This implementation can be used to realize bilateral microstrip circuits and ultimately allows more compact circuit integration. The DR is positioned on a substrate supported by a perfect electric conductor (PEC) ground plane with a slot aperture. On the other side of the PEC ground plane, a microstrip line is extended to the area beneath the slot. The DR is excited by coupling through the slot to the microstrip line where the source voltage is applied. Again, after applying the equivalence principle at the slot, the original problem can be divided into two equivalent situations. Fig. 4(b) illustrates the equivalent problem valid in the upper half-space $z > 0$. This problem is similar to the problem of DR with direct excitation, except for the presence of the equivalent magnetic current $\mathbf{J}^{m+}$ just above the original slot area. It should be understood that the physical slot has been shorted in the equivalent problem. Fig. 4(c) illustrates the equivalent problem valid in the lower half-space $z < 0$. This problem is a typical microstrip-line problem, except, of course, that the physical slot has been replaced by the equivalent magnetic current $\mathbf{J}^{m-}$. According to the boundary condition that the tangential component of the electric field is continuous across the slot, we have $\mathbf{J}^{m-} = -\mathbf{J}^{m+}$. The two equivalent problems are then coupled with each other by enforcing magnetic-field continuity across the slot, and a system of integral equations can be established to determine the unknown equivalent currents. This system of equations is given by (2), except that the electric fields on the microstrip conductor surface S_c should include a subscript L to denote that the parameters of the lower half-space are used, the exterior electric and magnetic fields on the DR surface S_d should include a subscript U to denote that the parameters of the upper half-space are used, and an equation must be included

to enforce continuity of the tangential magnetic field across the slot aperture surface S_a

$$\mathbf{H}_L^s|_{\tan} - \mathbf{H}_U^s|_{\tan} = 0, \qquad \text{on } S_a. \tag{25}$$

VI. Numerical Procedure

Here, the MoM [39] is employed in conjunction with the potential dyadic Green's functions given by (19) and (20) along with their duality counterparts to solve the DR microstrip circuit problem. In the numerical procedure, the triangular patch model developed in [13] is employed. The procedure is modified to handle the potential dyadic kernels and the dyadic charge density. As the first step of the numerical process, the surfaces of the objects embedded in the multilayered media are approximated by a set of planar triangular patches. The equivalent surface currents are then expanded using basis functions defined on triangle pairs with the unknown coefficients corresponding to the common edges. The charge density discontinuity that may exist at an interface is accounted for by the line integral in (11). Testing functions are then chosen to enforce the integral equations on each triangle pair, which reduces the integral equation into a system of linear equations or, in more compact form, a matrix equation. In order to extract the S-parameters of a multiport microstrip circuit, a matched-load simulation [4] is used, which results in modification of the Z-matrix. Once the matrix equation is solved, the S-parameters can be evaluated from the current standing-wave patterns.

A. Triangular Patch Model

Following the RWG procedure [13], the surface S of the object is modeled by planar triangular patches. The unknown current density is then expanded on triangle pairs as

$$\mathbf{J}(\mathbf{r}) = \sum_{n=1}^{N} I_n \mathbf{f}_n(\mathbf{r}) \tag{26}$$

where N is the number of interior edges and the I_n's are the unknown coefficients to be determined. After representing the basis function $\mathbf{f}_n$ associated with the nth edge in the local coordinate system [40], the dyadic charge density associated with the basis function can be written as

$$\begin{aligned}\nabla \mathbf{f}_n^{\pm} &= \pm \frac{1}{h_n}(\nabla \xi_{n+1} \mathbf{l}_{n-1} - \nabla \xi_{n-1} \mathbf{l}_{n+1}) \\ &= \mp \frac{1}{h_n}\left(\frac{1}{h_{n+1}}\hat{\mathbf{h}}_{n+1}\mathbf{l}_{n-1} - \frac{1}{h_{n-1}}\hat{\mathbf{h}}_{n-1}\mathbf{l}_{n+1}\right)\end{aligned} \tag{27}$$

where ξ_n's are the normalized area coordinates, $\mathbf{l}_n$'s are sequentially oriented vectors forming the triangle edges, and $\hat{\mathbf{h}}_n = \hat{\mathbf{l}}_n \times \hat{\mathbf{n}}$, h_n is the height of the triangle with respect to the nth edge, and the subscripts are counted modulo three (e.g., $l_0 \equiv l_3$ and $l_4 \equiv l_1$). Thus, as can be seen in (27), the dyadic charge density can be written in a simple form in terms of the parameters of the triangular patch.

B. Implementation of the MPIE

For the problem of a DR coupled to a microstrip line, upon using the expansion for the surface current densities in (26) and employing a Galerkin testing procedure, a partitioned matrix equation can be obtained as follows:

$$\begin{bmatrix} [Z_{ss}^{ee}] & [Z_{sd}^{ee}] & [Z_{sd}^{em}] \\ [Z_{ds}^{ee}] & [Z_{dd}^{ee}] & [z_{dd}^{em}] \\ [Z_{ds}^{me}] & [Z_{dd}^{me}] & [z_{dd}^{mm}] \end{bmatrix} \cdot \begin{bmatrix} [I_s^e] \\ [I_d^e] \\ [I_d^m] \end{bmatrix} = \begin{bmatrix} [V_s] \\ [\mathbf{0}] \\ [\mathbf{0}] \end{bmatrix} \tag{28}$$

where subscripts s and d denote, respectively, the microstrip line and DR, while the superscripts e and m denote, respectively, the electric field or current and magnetic field or current. The elements of $[Z_{ss}^{ee}]$, $[Z_{sd}^{ee}]$, $[Z_{ds}^{ee}]$, and $[Z_{dd}^{ee}]$ are given in terms of potential functions as

$$Z_{mn}^{ee} = l_m \left[j\omega \left(\mathbf{A}_{mn}^{+} \cdot \frac{\rho_m^{c+}}{2} + \mathbf{A}_{mn}^{-} \cdot \frac{\rho_m^{c-}}{2} \right) + \phi_{mn}^{e-} - \phi_{mn}^{e+} \right]. \tag{29}$$

The elements in $[Z_{ds}^{me}]$ and $[Z_{dd}^{me}]$ are given as

$$Z_{mn}^{me} = -l_m \left[\frac{1}{\mu} \left(\nabla \times \mathbf{A}_{mn}^{+} \cdot \frac{\rho_m^{c+}}{2} + \nabla \times \mathbf{A}_{mn}^{-} \cdot \frac{\rho_m^{c-}}{2} \right) \right]. \tag{30}$$

In (29) and (30), the potentials are given by

$$\begin{aligned}\mathbf{A}_{mn}^{\pm} &= \int\int_{s_n} \overline{\mathbf{K}}^A \cdot \mathbf{f}_n^{\pm}(\mathbf{r})\, ds' \pm (\hat{\mathbf{u}} \cdot \hat{\mathbf{z}})^2 \\ &\quad \cdot \int_{\partial s_n} \left[k_v^e(\mathbf{r}, \mathbf{r}') - k_h^e(\mathbf{r}, \mathbf{r}') \right] dl' \qquad (31a) \\ \phi_{mn}^{e\pm} &= \int\int_{s_n} \overline{\mathbf{G}}^e(\mathbf{r}, \mathbf{r}') : \nabla' \mathbf{f}_n^{\pm}(\mathbf{r}')\, ds'. \qquad (31b)\end{aligned}$$

The elements in $[Z_{sd}^{em}]$, $[Z_{dd}^{em}]$, and $[Z_{dd}^{mm}]$ are easily obtained in terms of the electric vector potential and the magnetic scalar potential by duality. Details are given in [22].

In the normalized area coordinates system, the magnetic vector potential $\mathbf{A}_{mn}^{\pm}$ associated with a pair of triangles can be represented as

$$\begin{aligned}\mathbf{A}_{mn}^{\pm} = l_m \Big[&\overline{\mathbf{I}}_1 \cdot (\mathbf{r}_2 - \mathbf{r}_1) + \overline{\mathbf{I}}_2 \cdot (\mathbf{r}_3 - \mathbf{r}_1) + \overline{\mathbf{I}} \cdot (\mathbf{r}_1 - \mathbf{r}_m) \Big] \\ &\pm (\hat{\mathbf{u}} \cdot \hat{\mathbf{z}})^2 \int_{\partial s_n} (k_v^e - k_h^e)\, dl'\end{aligned} \tag{32}$$

where

$$\begin{aligned}\overline{\mathbf{I}}_1 &= \int\int_{T_n} \xi_1 \overline{\mathbf{K}}^A\, d\xi_1\, d\xi_2 \\ \overline{\mathbf{I}}_2 &= \int\int_{T_n} \xi_2 \overline{\mathbf{K}}^A\, d\xi_1\, d\xi_2 \\ \overline{\mathbf{I}} &= \int\int_{T_n} \overline{\mathbf{K}}^A\, d\xi_1\, d\xi_2.\end{aligned}$$

After some manipulations, $\phi_{mn}^{e\pm}$ can be written as

$$\begin{aligned}\phi_{mn}^{e\pm} = \int\int_{T_n} \Big[&k_h^e \nabla' \cdot \mathbf{f}_n^{\pm} \mp \frac{1}{h_n}\, \hat{z}\hat{z} : \\ &\left(\frac{1}{h_{n+1}} \hat{\mathbf{h}}_{n+1} \mathbf{l}_{n-1} - \frac{1}{h_{n-1}} \hat{\mathbf{h}}_{n-1} \mathbf{l}_{n+1} \right) \\ &\cdot (k_v^e - k_h^e) \Big]\, d\xi_1\, d\xi_2.\end{aligned} \tag{33}$$

Similar equations in terms of normalized area coordinates for $\mathbf{F}_{mn}^{\pm}$ and $\phi_{mn}^{m\pm}$ can also be obtained. We observe, from (32),

that an undesirable line integral appears when objects penetrate interfaces. However, this line integral and the additional integral due to the second term of (33) are of scalar type and nonsingular. The extra effort in evaluating these integrals is well worth the cost in order to keep the three dyadic integrals in (32) in the simplest forms. For a planar microstrip circuit, $\hat{\mathbf{h}}_i$ and $\mathbf{l}_i$ are normal to $\hat{z}$, thus the second term of (33) disappears.

For the problem of a DR coupled to a slot aperture, upon using the expansion for the surface current densities in (2) and (25) and testing the resulting equations with $\mathbf{f}_n$, a partitioned matrix equation can be obtained of the form

$$\begin{bmatrix} [Z^{ee}_{ssL}] & [Z^{em}_{saL}] & [\mathbf{0}] & [\mathbf{0}] \\ [Z^{me}_{asL}] & [Z^{mm}_{aaL}+Z^{mm}_{aaU}] & [-Z^{me}_{adU}] & [Z^{mm}_{adU}] \\ [\mathbf{0}] & [-Z^{em}_{daU}] & [Z^{ee}_{ddU}] & [Z^{em}_{ddU}] \\ [\mathbf{0}] & [-Z^{mm}_{daU}] & [Z^{me}_{ddU}] & [Z^{mm}_{ddU}] \end{bmatrix} \cdot \begin{bmatrix} [I^e_s] \\ [I^m_a] \\ [I^e_d] \\ [I^m_d] \end{bmatrix} = \begin{bmatrix} [V_s] \\ [\mathbf{0}] \\ [\mathbf{0}] \\ [\mathbf{0}] \end{bmatrix} \quad (34)$$

where the subscripts s, a, and d denote, respectively, microstrip line, slot aperture, and DR, and the subscripts U and L denote, respectively, upper half-space and lower half-space, while the superscripts e and m denote, respectively, electric field or current and magnetic field or current. The elements of the Z-matrix are given by the same equations as those for the problem of a DR coupled to a microstrip line, provided that the corresponding upper or lower medium parameters are used.

Due to its dyadic nature, the implementation of the potential Green's functions is very tedious. However, the computational effort is greatly reduced since the kernels of these functions are the transmission-line voltages and currents that satisfy the transmission-line equations (A-5), and furthermore, by duality, $Y^p_{\tau\zeta}(z, z')$ and $T^p_{v\tau\zeta}(z, z')$ can be obtained by replacing all the characteristic impedances z^p with their reciprocal y^p (characteristic admittance) in $Z^p_{\tau\zeta}(z, z')$ and $T^p_{i\tau\zeta}(z, z')$, which results in changing the signs of all reflection coefficients. Also, in order to speed up the computation of the dyadic Green's functions, a general three-dimensional interpolation model has been developed [41]. The interpolation model selects M vertical planes to be tabulated and then interpolates between them. All the grid values on the same vertical plane can be tabulated by a single subroutine call, which saves the overhead due to the stack manipulations necessary for subroutine calls and the overhead due to the recomputation of the quadrature coefficients, the Bessel functions, and the transmission-line parameters.

VII. Circuit Parameter Extraction

A. Evaluation of the S-Parameters

The feed lines of a microstrip circuit support only hybrid electromagnetic (HEM) waves. For moderately low frequencies ($w \ll \lambda$ and $h \ll \lambda$), the HEM field has negligibly small longitudinal components [42]. With this quasi-TEM assumption, the traditional transmission-line theory can be used to evaluate the S-parameters of a multiport microstrip circuit as long as the reference planes are specified far from the discontinuities. This can be done by extending the physical lengths of the feed lines and exciting the input port with all output ports matched so that the incident, reflected, and transmitted waves can be identified. In the MoM procedure, the excitation can be modeled with a δ-gap voltage source, while the matched outputs can be simulated by enforcing in the space domain a unidirectional current traveling wave propagating in the direction away from the discontinuities. This procedure is known as matched load simulation (MLS). This simulation procedure results in the modification of matrix equations (28) and (34). Two simulation methods have been proposed in [4]. The first method enforces a traveling wave with amplitude equal to one on the output port, while it leaves the δ-gap voltage source to be determined. This method requires one to rearrange the matrix equation, and the rearrangement is quite tedious for a multiport network. The second method described below is more suitable for multiport microstrip circuits, thus, it is employed here. For a narrow output line, as shown in Fig. 5, if j denotes an edge where the traveling-wave constraint is to be enforced, the simulation can be done by introducing new linear equations into the matrix equation of the form

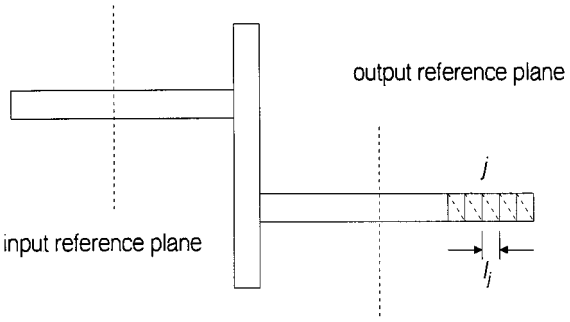

Fig. 5. Matched output port with MLS applied on the triangle edges denoted by solid lines.

$$I^e_{sj} - I^e_{s(j+1)} e^{-j\beta_g l_j} = 0 \quad (35)$$

where β_g is the transmission-line wavenumber, l_j is the length between edge j, and the next constraint edge. With the new linear equation, the jth row in the Z-matrix becomes

$$[0 \quad \cdots \quad 1 \quad -e^{-j\beta_g l_j} \quad 0 \quad \cdots \quad 0]. \quad (36)$$

Once the modified matrix equation is solved for the current distribution, the S-parameters can be extracted from the current standing-wave patterns.

B. Q Circles

The equivalent circuit for a $\mathrm{TE}_{01\delta}$ mode coupled to a microstrip line is shown in Fig. 6. The loci of z_{in} for different values of d form one or more distinct circles on the Smith chart, where z_{in} is the normalized impedance in the symmetry pp' plane, and d is the distance from the edge of the DR to the edge of the microstrip line. These loci are called Q circles [43]. For a high-Q resonator circuit, the loci move considerably faster in the vicinity of the resonant frequency. For a particular value of

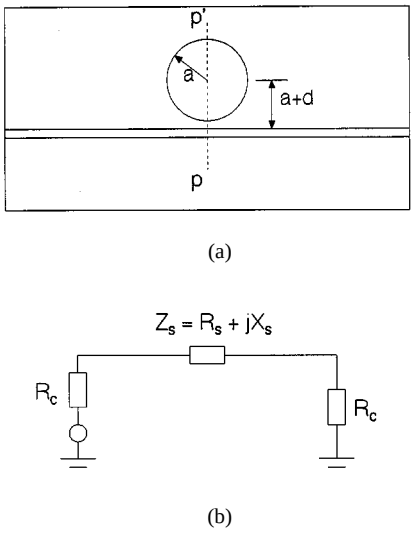

Fig. 6. Equivalent circuit of a $\mathrm{TE}_{01\delta}$-mode resonator coupled to a microstrip line. (a) Actual configuration. (b) Equivalent circuit.

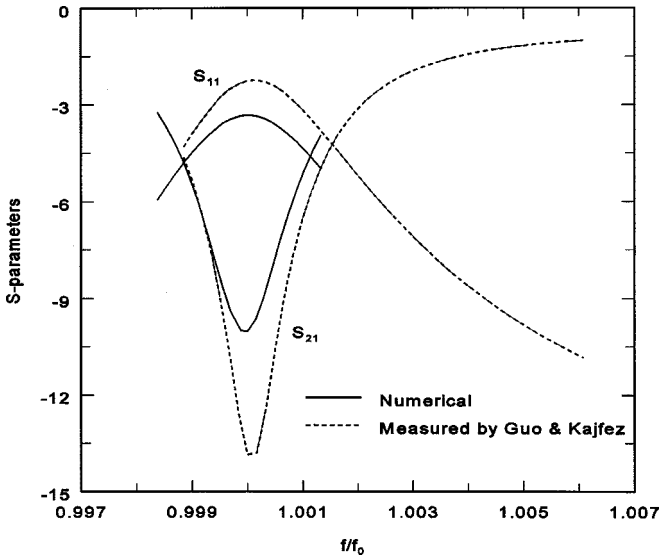

Fig. 7. S-parameters of a $\mathrm{TE}_{01\delta}$-mode resonator coupled to a microstrip line with $d = 0$.

d, the diameter d_c of a Q circle determines the coupling coefficient

$$\kappa = \frac{d_c}{2 - d_c}. \tag{37}$$

Critical coupling $(\kappa = 1)$ occurs when the diameter of the Q circle is equal to one. For this case, the power dissipated in the resonator is equal to the power delivered to the external circuit. The loaded quality factor can be determined by the following equation:

$$Q_L = \frac{1}{2} \frac{f_0}{f_2 - f_1} (\tan\phi_2 - \tan\phi_1) \tag{38}$$

where f_0 is the resonant frequency, f_1 and f_2 are the frequencies corresponding to the preselected angles ϕ_1 and ϕ_2 counted clockwise and anticlockwise from $\phi = 0$ at the resonant frequency.

VIII. Numerical Results

For validation, several examples have been computed for planar microstrip circuits, such as the filter example in [4] and the microstrip line coupler in [44], but these results are omitted for brevity. The example of a dipole antenna penetrating a half-space dielectric interface with an angle was also considered, and our results were found to be in agreement with those published in [45]. These results are presented in [41].

A. DR Coupled to a Microstrip Circuit

The traditional way of coupling a DR to a microstrip circuit is to place the DR beside a microstrip line that is connected to the microstrip circuit. A theoretical study of such a DR coupled to a microstrip line is first conducted. The numerical results are then compared to available measured data [28]. A novel tuning mechanism [38] is also investigated numerically. The second case studied in this section is a microstrip-line aperture-coupled DR antenna. Numerical results for this case are computed with the approach presented here and are compared with available measured data [46]. All the numerical computations are performed with the Trans-Tech resonator made of D8600 material $(\epsilon_r = 80)$, and having a diameter of 22.99 mm and a height of 10.34 mm.

1) DR Coupled to a Microstrip Line: The geometry and the equivalent circuit for coupling of the $\mathrm{TE}_{01\delta}$ resonator mode to a microstrip line are shown in Fig. 6. The substrate is Rogers RT/Duroid 5880 of thickness 1.59 mm and the relative dielectric constant is 2.2. The width of the microstrip line is chosen to be 4.8 mm to achieve a 50-Ω characteristic impedance. This structure has been previously investigated experimentally by Kajfez and Guo [28]. Numerical results are computed for comparison. In the numerical procedure, the microstrip line is extended to identify the incident and reflected waves, and the DR is modeled with 880 triangles. On the bottom and the top of the dielectric cylinder, four triangles are employed for the innermost circles, while 64 triangles are used for the outermost rings.

The coupling coefficient and the loaded Q factor can be regulated by changing the distance between the DR and microstrip line. For $d = 0$ mm, the numerical results for the S-parameters are shown as functions of relative frequency f/f_0 in Fig. 7. The computed resonant frequency is $f_0 = 1.6928$ GHz, while the measured one is $f_0 = 1.7037$ GHz, thus, the difference in the resonant frequency is 0.64%. The standing-wave patterns for the current at three different frequencies on the microstrip line are shown in Fig. 8. One observes from Fig. 8 that the current distributions remain approximately constant at the output port due to the effect of the matched load, while they vary significantly at the input port due to the equivalent impedance Z_s at $L = 0$.

For cases in which d is varied from 0 to 6 mm, the computed and measured resonant frequencies, as well as the percentage differences between them, are summarized in Table I. The computed coupling coefficients and the Q factors are computed by the program QZERO in [43]. The results are summarized in Table II.

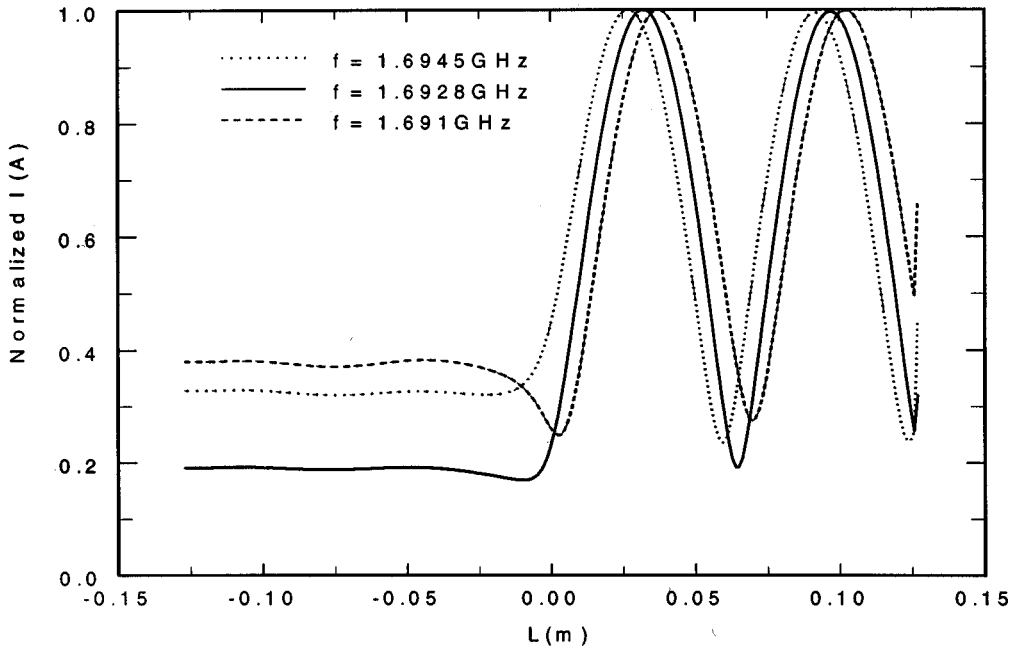

Fig. 8. Current distributions on the microstrip line.

TABLE I
RESONANT FREQUENCIES

d (mm)	Numerical f_0 (GHz)	Measured f_0 (GHz)	Δ
0	1.6928	1.7037	0.64%
1	1.69255	1.70336	0.63%
2	1.6923	1.7029	0.62%
3	1.69215	1.7026	0.61%
4	1.69207	1.7024	0.61%
5	1.6920	1.7022	0.60%
6	1.6919	1.7020	0.59%

B. Tuning DR

A novel tuning mechanism introduced by Buer and El-Sharawy [38] is investigated numerically next. The technique, as shown in Fig. 9, employs a nonresonant section of a microstrip line to modify the resonant frequency. The reactance added to the resonator can be adjusted by simply changing the offset s of the tuning line with respect to the center of the DR. A nonresonant tuning line was employed to avoid significant Q degradation, although it provides less tuning range than a resonant line does. In the numerical computation, DRs with both nonresonant and resonant tuning lines are investigated. The nonresonant and resonant tuning lines are of lengths $l_t = 96.75$ mm (approximately $3/4\lambda_g$ at $s = 0$) and $l_t = 62.5$ mm (approximately $1/2\lambda_g$ at $s = 0$), respectively, and both are of characteristic impedance $R_0 = 50\,\Omega$ with both ends open. The parameters of the DR, microstrip feed line, and substrate are the same as in the previous case. For a DR with a nonresonant tuning line, the numerical results for the equivalent series impedance Z_s for different values of s are shown in Fig. 10 and the variation of the resonant frequency and the unloaded quality factor as a function of the offset s are shown in Table III. For a DR with a resonant tuning line, the numerical results for the equivalent series impedance Z_s for different values of s are shown in Fig. 11 and the variation of the resonant frequency and the unloaded quality factor as a function of the offset s are shown in Table IV. It can be seen, from Tables III and IV, that the unloaded quality factor of a DR with a resonant tuning line is much smaller than that of a DR with a nonresonant tuning line. That is because the radiation loss of the former is much larger than that of the latter.

C. DR Coupled to a Slot Aperture

The geometry for coupling of the $\mathrm{HEM}_{11\delta}$ resonator mode to a slot aperture is shown in Fig. 4(a). The substrate on which the microstrip line is etched is Rogers RT/Duroid 5880 of thickness 1.575 mm and the relative dielectric constant is 2.2 with

TABLE II
COUPLING COEFFICIENTS AND Q FACTOR

	Numerical				Measured			
d(mm)	Q_l	κ	Q_0	Q_{ex}	Q_l	κ	Q_0	Q_{ex}
0	266	2.13	831	390	297	4.65	1679	361
1	327	1.48	812	549	391	2.99	1561	522
2	392	1.07	811	758	507	1.96	1502	765
3	453	0.775	803	1036	617	1.30	1420	1092
4	511	0.570	803	1409	717	0.998	1433	1436
5	560	0.428	800	1869	810	0.740	1410	1904
6	595	0.323	788	2440	920	0.524	1402	2677

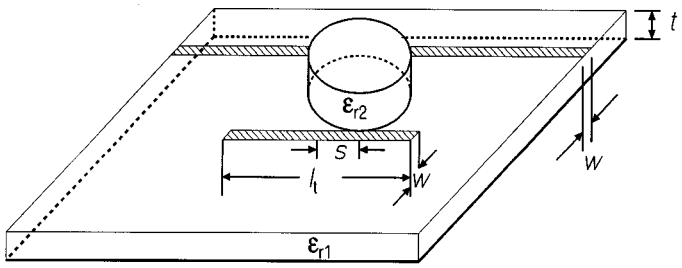

Fig. 9. Tuning DR.

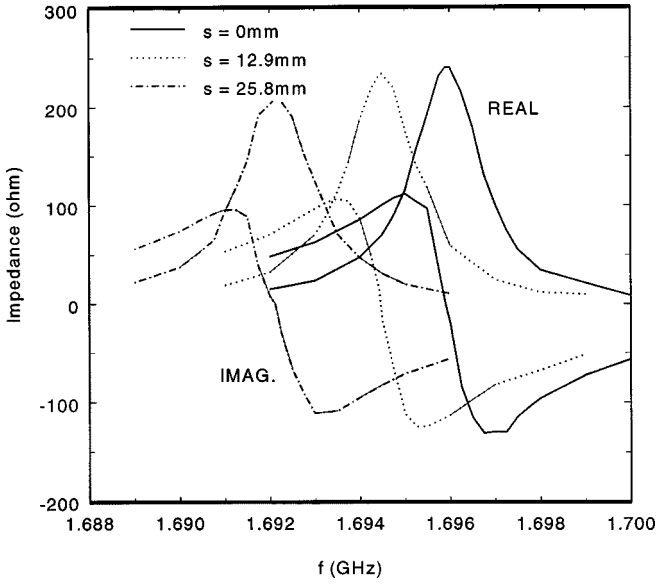

Fig. 10. Z_s of a DR with nonresonant tuning line as a function of frequency for $s = 0$, $s = 12.9$ mm, and $s = 25.8$ mm.

loss tangent 0.0004. The width of the microstrip line is chosen to be 4.5 mm to achieve a 50-Ω characteristic impedance. The parameters of the DR are the same as in the two previous cases. The ground plane has a 23 $\times$ 2 mm rectangular aperture that provides the excitation for the $\mathrm{HEM}_{11\delta}$ mode in the DR. This structure is primarily used as an antenna to achieve wider bandwidth and higher power-handling capability, as compared with microstrip antenna of similar size.

TABLE III
RESONANT FREQUENCY AND UNLOADED Q FACTOR OF A DR WITH NONRESISTANT TUNING LINE

s (mm)	Resonant frequency (GHz)	Unloaded Q factor
0	1.6959	939
6.45	1.69565	926
12.9	1.6944	892
19.35	1.6932	896
25.8	1.69212	822
32.25	1.6916	805

TABLE IV
RESONANT FREQUENCY AND UNLOADED Q FACTOR OF A DR WITH A RESONANT TUNING LINE

s (mm)	Resonant frequency (GHz)	Unloaded Q factor
0	1.6959	448
6.45	1.69565	429
12.9	1.6944	433
19.35	1.6932	436
25.8	1.69212	450
32.25	1.6916	477

The resonant frequency and input resistance of the $\mathrm{HEM}_{11\delta}$ mode can be controlled by changing the thickness and permittivity of the substrate on which the DR resides. For the case in which $t_d = 0.79$ mm with $\epsilon_{rd} = 2.5$, the numerical results for the series equivalent impedance Z_s are shown in Fig. 12 and the numerical results are compared with measured data from [46]. The measurement was performed on the same geometry, except that the substrate on which the DR resided was replaced by a dielectric spacer of diameter 22.99 mm with the same permittivity and thickness. As can be seen, reasonable agreement has been obtained. A possible reason for the differences could be due to the infinite ground-plane model and the surface waves that are excited in the numerical models. The surface waves are absent in the measurement model because the substrate (a spacer) does not extend beyond the DR. It should be noted that the resonant

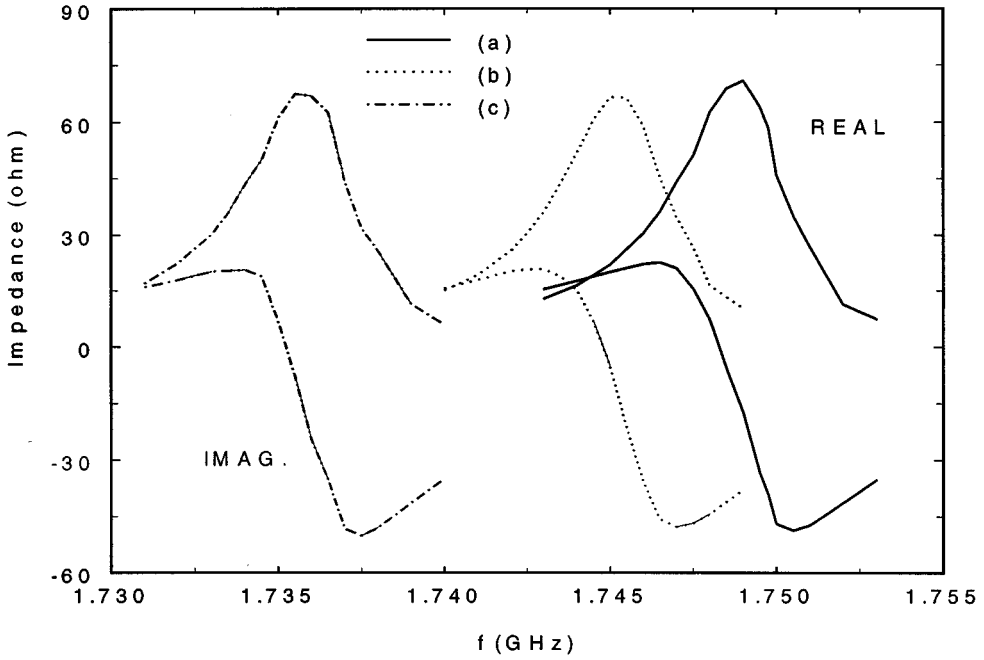

Fig. 11. Z_s of a DR with a resonant tuning line as a function of frequency for $s = 0$, $s = 6.45$ mm, $s = 12.9$ mm. (a) $s = 0$. (b) $s = 6.45$ mm. (c) $s = 12.9$ mm.

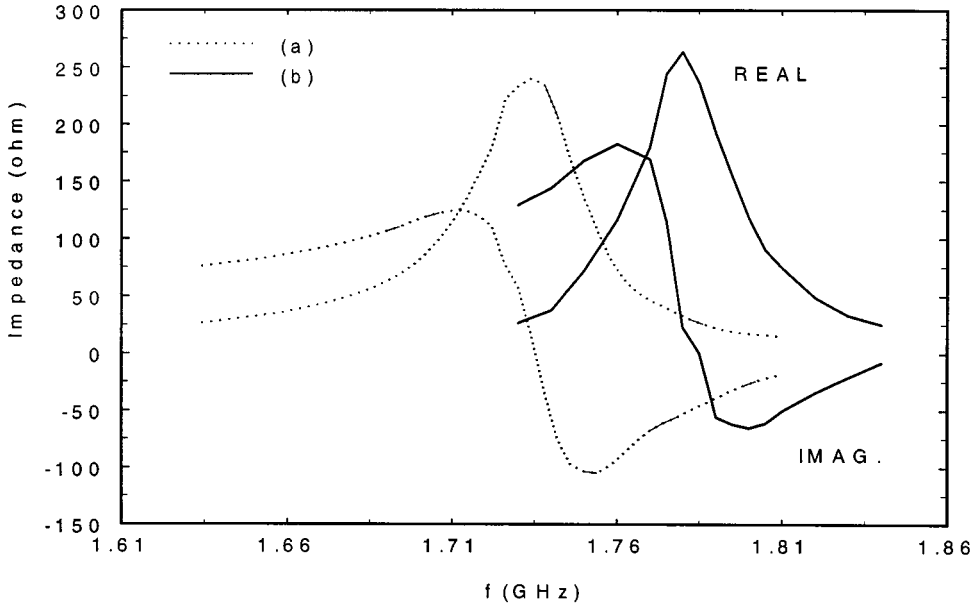

Fig. 12. Z_s of an $\mathrm{HEM}_{11\delta}$-mode resonator coupled to a slot aperture ($t_d = 0.79$ mm, $\epsilon_{rd} = 2.5$). (a) Measured data from [46]. (b) This method.

frequency obtained with the numerical model is within 3% of the measured result.

For the case in which ϵ_{rd} is varied from 2 to 2.5, results for the series equivalent impedance Z_s as a function of frequency are shown in Fig. 13. As the permittivity of the substrate on which the DR resides increases, the electrical length of the slot increases, thus, the $\mathrm{HEM}_{11\delta}$ mode is more strongly coupled. For the cases in which t_d is varied from 0.79 to 1.59 mm, results for the series equivalent impedance Z_s as a function of frequency are shown in Fig. 14.

IX. Conclusion

In this paper, a new MPIE formulation has been developed for the analysis of electromagnetic problems due to conducting or dielectric objects of arbitrary shape embedded in a planarly stratified medium. In the new MPIE formulation, the dyadic kernel of the vector potential is kept in the simple form originally developed by Sommerfeld, yet the scalar potential, which is represented by a double-dot product of a dyadic kernel with a dyadic charge density, remains compatible with the original

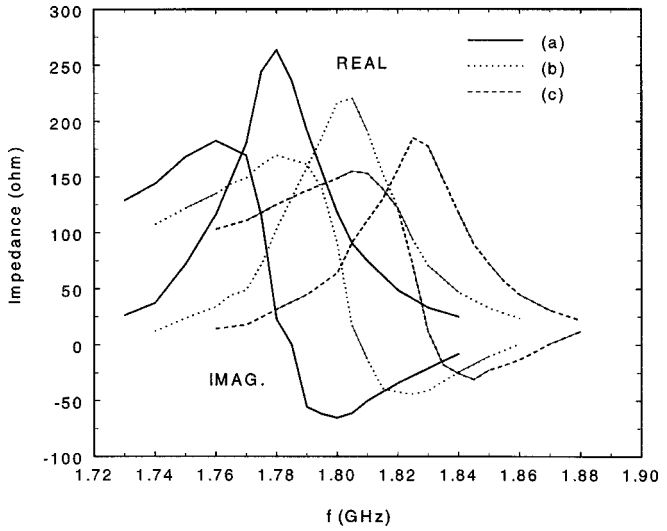

Fig. 13. Z_s of an $\mathrm{HEM}_{11\delta}$-mode resonator coupled to a slot aperture ($t_d = 0.79$ mm). (a) $\epsilon_{rd} = 2.5$. (b) $\epsilon_{rd} = 2.25$. (c) $\epsilon_{rd} = 2.0$.

triangular patch implementation. When it is represented in the local coordinate system, the dyadic charge density can be written in a simple form in terms of the orientation and shape of the triangle. Thus, the numerical implementation of the double-dot product is trivial if one takes advantage of the well-established basis functions in which the unknown current density is expressed. This new MPIE formulation is valid for electromagnetic problems in an inhomogeneous and/or anisotropic medium, provided that the correct dyadic kernel is employed. As presented in [48], the E- and H-field dyadic Green's functions have been derived for many classical electromagnetic boundary problems. However, the potential dyadic Green's functions for most of these problems still remain unknown. The new MPIE formulation is derived from the E- and H-field dyadic Green's functions based on a general expression of the vector-potential dyadic Green's function. Thus, once the E- and H-field dyadic Green's functions are available, the derivation procedure for the MPIE formulation presented in this paper can be applied for many of these boundary problems. In summary, the derivation of the new MPIE formulation is systematic and the numerical implementation is efficient, yet it remains compatible with the original procedure.

The new MPIE formulation has been employed in conjunction with the triangular patch model, originally developed for arbitrarily shaped objects in free space [13] to solve a DR microstrip circuit problem. The numerical procedure has been modified to handle the dyadic kernels of the potentials and the dyadic charge density. In order to extract the S-parameters of a DR microstrip circuit, an MLS [4] has been used, which results in modification of the Z-matrix. Once the matrix equation is solved, the S-parameters can be evaluated from the current standing-wave patterns. The diameters of the Q circles have been measured to determine the coupling coefficients and the Q factors of the DR excited by a microstrip circuit. The numerical results of current distributions, S-parameters, and equivalent serial impedances for a $\mathrm{TE}_{01\delta}$-mode DR coupled to a microstrip line and an $\mathrm{HEM}_{11\delta}$-mode DR coupled to a slot aperture have been presented and discussed. The coupling coefficient and Q factor of the $\mathrm{TE}_{01\delta}$-mode DR have also been evaluated. The validity of the new MPIE formulation and the numerical procedure have been verified by comparing the obtained S-parameters with available measurement data. It is worthwhile to mention that, as demonstrated by the cases of a thin-wire antenna partially buried in the earth and sea [41], [45], [47], the new MPIE formulation and the numerical procedure are valid and well suited for objects penetrating an interface between two media.

Appendix
General Form of Vector-Potential Dyadic Green's Functions

In an anisotropic space, different field components are, in general, coupled together, which makes the solution extremely tedious. Fortunately, in a uniaxial stratified media, the longitudinal- and transverse-field components can be decoupled. By expanding the transverse fields into modal functions, the transverse-field equations can be reduced to two simple transmission-line equations along the z-direction. One of them is for the TE modes, the other is for the TM modes.

The modal functions $\mathbf{e}_{tn}$ and $\mathbf{h}_{tn}$ must be complete and orthogonal to each other. They represent TE_z and TM_z components, respectively. The orthogonality of $\mathbf{e}_{tn}$ and $\mathbf{h}_{tn}$ can be expressed as

$$\begin{cases} \mathbf{e}_{tn} \times \hat{\mathbf{z}} = \mathbf{h}_{tn} \\ \hat{\mathbf{z}} \times \mathbf{h}_{tn} = \mathbf{e}_{tn} \end{cases} \quad \text{and } \langle \mathbf{e}_{tn}, \mathbf{e}^*_{tn} \rangle = \langle \mathbf{h}_{tn}, \mathbf{h}^*_{tn} \rangle = 1 \ . \tag{A-1}$$

The completeness criterion is guaranteed if one of them is solenoidal and the other is irrotational [36] as follows:

$$\begin{cases} \nabla \times \mathbf{e}_{tn} = 0 \\ \nabla \cdot \mathbf{h}_{tn} = 0. \end{cases} \tag{A-2}$$

For a planarly stratified structure, cylindrical vector wave functions are good candidates. The transverse components of the solenoidal functions satisfy (A-1) and (A-2), as is proven in [22, App. C].

The transmission-line equations for the expansion coefficients V_n and I_n in either the TE or TM case can be derived as [36, p. 747]

$$-\frac{dV_n(z)}{dz} = -jk_{z\tau} z_\tau I_n(z) + v_n(z) \tag{A-3a}$$

$$-\frac{dI_n(z)}{dz} = -jk_{z\tau} y_\tau V_n(z) + i_n(z) \tag{A-3b}$$

where, for TM modes, the propagation constant k_z and the characteristic impedance z_τ are defined as

$$\begin{aligned} z^e_\tau &= \frac{1}{y^e_\tau} = \frac{k^e_{z\tau}}{\omega \epsilon_{t\tau}} \\ k^e_{z\tau} &= \sqrt{\frac{\epsilon_{t\tau}}{\epsilon_{z\tau}}} \sqrt{k_{1\tau}^2 - k_\rho^2} \\ k_{1\tau}^2 &= \omega^2 \mu_{t\tau} \epsilon_{z\tau} \end{aligned} \tag{A-4a}$$

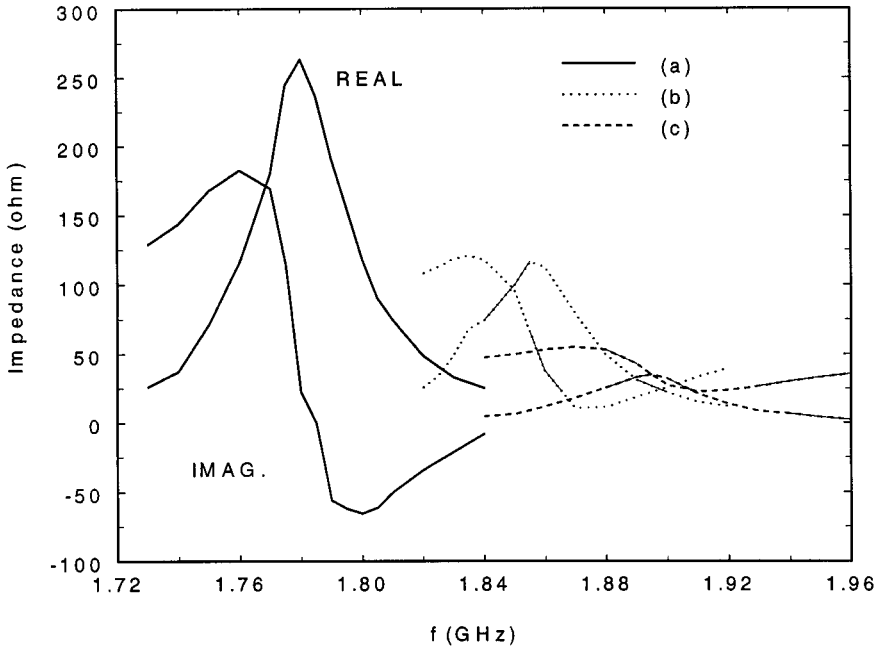

Fig. 14. Z_s of an $\mathrm{HEM}_{11\delta}$-mode resonator coupled to a slot aperture ($\epsilon_{rd} = 2.5$). (a) $t_d = 0.79$ mm. (b) $t_d = 1.19$ mm. (c) $t_d = 1.59$ mm.

while for TE modes

$$z_\tau^h = \frac{1}{y_\tau^h} = \frac{\omega\mu_{t\tau}}{k_{z\tau}^h}$$
$$k_{z\tau}^h = \sqrt{\frac{\mu_{t\tau}}{\mu_{z\tau}}}\sqrt{k_{2\tau}^2 - k_\rho^2}$$
$$k_{2\tau}^2 = \omega^2\epsilon_{t\tau}\mu_{z\tau}. \tag{A-4b}$$

In order to solve the transmission-line equations (A-3) for the voltage $V(z)$ and current $I(z)$, it is convenient to introduce the voltage and current transmission-line Green's functions, which are defined as

$$-\frac{dT_{v\tau\varsigma}^p(z, z')}{dz} = -jk_{z\tau}^p z_\tau^p Y_{\tau\varsigma}^p(z, z') - \delta(z - z') \tag{A-5a}$$
$$-\frac{dY_{\tau\varsigma}^p(z, z')}{dz} = -jk_{z\tau}^p y_\tau^p T_{v\tau\varsigma}^p(z, z') \tag{A-5b}$$
$$-\frac{d}{dz} Z_{\tau\varsigma}^p(z, z') = -jk_{z\tau}^p z_\tau^p T_{i\tau\varsigma}^p(z, z') \tag{A-5c}$$
$$-\frac{d}{dz} T_{i\tau\varsigma}^p(z, z') = -jk_{z\tau}^p y_\tau^p Z_{\tau\varsigma}^p(z, z') - \delta(z - z') \tag{A-5d}$$

where the superscript p denotes e or h, while the subscripts τ and ς denote the observation and source layers, respectively. $Z_{\tau\varsigma}^p(z, z')$ and $T_{v\tau\varsigma}^p(z, z')$ denote the voltage Green's functions due to the current source $i^p(z')$ and the voltage source $v^p(z')$, respectively. $T_{i\tau\varsigma}^p(z, z')$ and $Y_{\tau\varsigma}^p(z, z')$ denote the current Green's functions due to the current source $i^p(z')$ and the voltage source $v^p(z')$, respectively.

The transmission-line Green's functions defined in (A-5) satisfy reciprocity properties when k_z^p and z^p are either constant or z dependent [36, p. 194]

$$Z_{\tau\varsigma}^p(z, z') = Z_{\varsigma\tau}^p(z', z) \tag{A-6a}$$
$$Y_{\tau\varsigma}^p(z, z') = Y_{\varsigma\tau}^p(z', z) \tag{A-6b}$$
$$T_{i\tau\varsigma}^p(z, z') = -T_{v\varsigma\tau}^p(z', z). \tag{A-6c}$$

The derivation of $Z_{\tau\varsigma}^p(z, z')$ has been conducted in [12], [36]. Once it is known, the remaining three transmission-line Green's functions can be found from (A-5) and (A-6) immediately. The E- and H-field dyadic Green's functions can be easily found in terms of the transmission-line Green's functions. From Maxwell's equations and the Lorenz gauge, a general expression of the dyadic Green's function for the magnetic vector potential in a uniaxial medium can be written as

$$\overline{\mathbf{G}}^A = G_{tt}^A\hat{\mathbf{t}}\hat{\mathbf{t}} + G_{zt}^A\hat{\mathbf{z}}\hat{\mathbf{t}} + G_{zz}^A\hat{\mathbf{z}}\hat{\mathbf{z}} \tag{A-7}$$

where the subscript t denotes components in the plane perpendicular to $\hat{\mathbf{z}}$.

Based on the expression of (A-7), a general form of the magnetic vector-potential dyadic can be derived from the field counterparts as

$$\begin{aligned}\overline{\mathbf{G}}^A = &-\int_0^\infty \frac{1}{k_\rho}\sum_n \frac{1}{(1+\delta_0)\pi}\frac{1}{j\omega} \\ &\cdot Z_{\tau\varsigma}^h(z, z')\mathbf{m}_{tn}(\rho)\mathbf{m}_{tn}^*(\rho')\,dk_\rho \\ &-\int_0^\infty \frac{1}{k_\rho}\sum_n \frac{1}{(1+\delta_0)\pi}\frac{k_0^2\mu_{t\tau}'\epsilon_{z\tau}'}{j\omega k_\rho^2}\frac{z_\tau^e}{v_{\epsilon\tau}} \\ &\cdot T_{i\tau\varsigma}^e(z, z')\mathbf{n}_{zn}(\rho)\mathbf{n}_{tn}^*(\rho')\,dk_\rho \\ &+\int_0^\infty \frac{1}{k_\rho}\sum_n \frac{1}{(1+\delta_0)\pi}\frac{k_0^2\mu_{t\tau}'\epsilon_{z\tau}'}{j\omega k_\rho^2}\frac{z_\tau^e z_\varsigma^e}{v_{\epsilon\tau}v_{\epsilon\varsigma}} \\ &\cdot Y_{\tau\varsigma}^e(z, z')\mathbf{n}_{zn}(\rho)\mathbf{n}_{zn}^*(\rho')\,dk_\rho.\end{aligned} \tag{A-8a}$$

Similarly, a general expression of the electric vector-potential dyadic Green's function can be written as

$$\begin{aligned}\overline{\mathbf{G}}^F = &-\int_0^\infty \frac{1}{k_\rho}\sum_n \frac{1}{(1+\delta_0)\pi}\frac{1}{j\omega} \\ &\cdot Y^e_{\tau\varsigma}(z,z')\mathbf{m}_{tn}(\rho)\mathbf{m}^*_{tn}(\rho')\,dk_\rho \\ &-\int_0^\infty \frac{1}{k_\rho}\sum_n \frac{1}{(1+\delta_0)\pi}\frac{k_0^2\epsilon'_{t\tau}\mu'_{z\tau}}{j\omega k_\rho^2}\frac{y^h_\tau}{v_{\mu\tau}} \\ &\cdot T^h_{v\tau\varsigma}(z,z')\mathbf{n}_{zn}(\rho)\mathbf{n}^*_{tn}(\rho')\,dk_\rho \\ &+\int_0^\infty \frac{1}{k_\rho}\sum_n \frac{1}{(1+\delta_0)\pi}\frac{k_0^2\epsilon'_{t\tau}\mu'_{z\tau}}{j\omega k_\rho^2}\frac{y^h_\tau y^h_\varsigma}{v_{\mu\tau}v_{\mu\varsigma}} \\ &\cdot Z^h_{\tau\varsigma}(z,z')\mathbf{n}_{zn}(\rho)\mathbf{n}^*_{zn}(\rho')\,dk_\rho \qquad \text{(A-8b)}\end{aligned}$$

where

$$\mathbf{n}_z(\rho) = n_z(\rho)\hat{\mathbf{z}}. \qquad \text{(A-9)}$$

It is worth noting that $\mathbf{n}_n(\rho)$ is also a function of k_z. In a uniaxial medium, k_z^e and k_z^h are, in general, not identical as indicated by (A-4). Since $\mathbf{n}_n(\rho)$ represents a TM wave, k_z^e is assumed unless an explicit expression is given as $\mathbf{n}_n(\rho, k_z^h)$.

ACKNOWLEDGMENT

The authors wish thank Prof. D. Kajfez, Department of Electrical Engineering, University of Mississippi, University, and Dr. J. Guo, Federal Express, Memphis, TN, for providing the measured results for the DR excited by a microstrip line and slot.

REFERENCES

[1] P. B. Katehi and N. G. Alexopoulos, "Frequency-dependent characteristics of microstrip discontinuities in millimeter-wave integrated circuits," *IEEE Trans. Microwave Theory Tech.*, vol. MTT-33, pp. 1029–1035, Oct. 1985.

[2] L. P. Dunleavy and P. B. Katehi, "A generalized method for analyzing thin microstrip discontinuities," *IEEE Trans. Microwave Theory Tech.*, vol. 36, pp. 1758–1766, Dec. 1988.

[3] F. Alonso-Monferrer, A. A. Kishk, and A. W. Glisson, "Green's functions analysis of planar circuits in a two-layer grounded medium," *IEEE Trans. Antennas Propagat.*, vol. 40, pp. 690–696, June 1992.

[4] E. K. L. Yeung, J. C. Beal, and Y. M. M. Antar, "Multilayer microstrip structure analysis with matched load simulation," *IEEE Trans. Microwave Theory Tech.*, vol. 43, pp. 143–149, Jan. 1995.

[5] G. V. Eleftheriades and J. R. Mosig, "On the network characterization of planar passive circuits using the method of moments," *IEEE Trans. Microwave Theory Tech.*, vol. 44, pp. 438–445, Mar. 1996.

[6] T. Itoh and R. Mittra, "Spectral-domain approach for calculating the dispersion characteristics of microstrip lines," *IEEE Trans. Microwave Theory Tech.*, vol. MTT-21, pp. 496–499, July 1973.

[7] N. K. Das and D. M. Pozar, "A generalized spectral-domain Green's function for multilayer dielectric substrates with application to multilayer transmission lines," *IEEE Trans. Microwave Theory Tech.*, vol. MTT-35, pp. 326–335, Mar. 1987.

[8] ——, "Full-wave spectral domain computation of material, radiation, and guided wave losses in infinite multilayered printed transmission lines," *IEEE Trans. Microwave Theory Tech.*, vol. 39, pp. 54–63, Jan. 1991.

[9] T. S. Horng, W. E. McKinzie, and N. G. Alexopoulos, "Full-wave spectral-domain analysis of compensation of microstrip discontinuities using triangular subdomain functions," *IEEE Trans. Microwave Theory Tech.*, vol. 40, pp. 2137–2147, Dec. 1992.

[10] K. A. Michalski, "The mixed-potential electric field integral equation for objects in layered media," *Arch. Elektron. Uebertrag.*, vol. 39, pp. 317–332, Sept.–Oct. 1985.

[11] ——, "On the scalar potential of a point charge associated with a time-harmonic dipole in a layered medium," *IEEE Trans. Antennas Propagat.*, vol. AP-35, pp. 1299–1301, Nov. 1987.

[12] K. A. Michalski and D. Zheng, "Electromagnetic scattering and radiation by surfaces of arbitrary shape in layered media—Part I: Theory," *IEEE Trans. Antennas Propagat.*, vol. 38, pp. 335–344, Mar. 1990.

[13] S. M. Rao, D. R. Wilton, and A. W. Glisson, "Electromagnetic scattering by surfaces of arbitrary shape," *IEEE Trans. Antennas Propagat.*, vol. AP-30, pp. 409–418, May 1982.

[14] J. R. Mosig, "Arbitrarily shaped microstrip structures and their analysis with a mixed potential integral equation," *IEEE Trans. Microwave Theory Tech.*, vol. 36, pp. 314–323, Feb. 1988.

[15] G. A. E. Vandenbosch and A. R. Van de Capelle, "Mixed- potential integral expression formulation of the electric field in a stratified dielectric medium—Application to the case of a probe current source," *IEEE Trans. Antennas Propagat.*, vol. 42, pp. 806–817, July 1992.

[16] K. A. Michalski and J. R. Mosig, "Multilayered media Green's functions in integral equation formulations," *IEEE Trans. Antennas Propagat.*, vol. 45, pp. 508–519, Mar. 1997.

[17] N. W. Montgomery and D. R. Wilton, "Analysis of arbitrary conducting period structures embedded in layered media," in *IEEE AP-S Int. Symp. Dig.*, London, ON., Canada, June 1991, pp. 1889–1892.

[18] D. R. Wilton, "Review of current status and trends in the use of integral equations in computational electromagnetics," *Electromag.*, vol. 12, pp. 287–341, July–Dec. 1992.

[19] J. Chen, A. A. Kishk, and A. W. Glisson, "MPIE for conducting sheets penetrating a multilayer medium," in *IEEE AP-S Int. Symp. Dig.*, Seattle, WA, June 1994, pp. 1346–1349.

[20] A. Sommerfeld, "Über die ausbreitung der wellen in der drahtlosen telegraphie," *Ann. Phys.*, vol. 4, no. 28, pp. 665–736, Jan. 1909.

[21] W. Zheng, "Wire antennas above and protruding through an air/lossy medium interface," Ph.D. dissertation, Dept. Elect. Eng., Univ. Mississippi, University, MS, 1995.

[22] J. Chen, "Full wave analysis of a dielectric resonator embedded in a uniaxial multilayered medium coupled to a microstrip circuit," Ph.D. dissertation, Dept. Elect. Eng., Univ. Mississippi, University, MS, 1996.

[23] P. Kaveh and A. H. Levesque, *Wireless Information Networks*. New York: Wiley, 1995.

[24] D. Kajfez and P. Guillon, *Dielectric Resonators*. Oxford, MS: Vector Fields, 1990.

[25] L. E. Larson, *RF and Microwave Circuit Design for Wireless Communications*. Norwood, MA: Artech House, 1996.

[26] A. Podcameni and L. F. M. Conrado, "Design of microwave oscillators and filters using transmission-mode dielectric resonators coupled to microstrip lines," *IEEE Trans. Microwave Theory Tech.*, vol. MTT-33, pp. 1329–1332, Dec. 1985.

[27] A. M. Pavio and M. A. Smith, "A 20-40-GHz push–push dielectric resonator oscillator," *IEEE Trans. Microwave Theory Tech.*, vol. MTT-33, pp. 1346–1349, Dec. 1985.

[28] D. Kajfez and J. Guo, "Precision measurement of coupling between microstrip and $\mathrm{TE}_{01\delta}$ mode dielectric resonator," *Electron. Lett.*, vol. 30, pp. 1772–1773, Oct. 1994.

[29] A. W. Glisson, D. Kajfez, and J. James, "Evaluation of modes in dielectric resonators using a surface integral equation formulation," *IEEE Trans. Microwave Theory Tech.*, vol. MTT-31, pp. 1023–1029, Dec. 1983.

[30] D. Kajfez, A. W. Glisson, and J. James, "Computed modal field distributions for isolated dielectric resonators," *IEEE Trans. Microwave Theory Tech.*, vol. MTT-32, pp. 1609–1616, Dec. 1984.

[31] G. P. Junker, "Analysis of dielectric resonator antennas excited by a coaxial probe or narrow slot aperture," Ph.D. dissertation, Dept. Elect. Eng., Univ. Mississippi, University, MS, 1994.

[32] G. P. Junker, A. A. Kishk, and A. W. Glisson, "Input impedance of dielectric resonator antennas excited by a coaxial probe," *IEEE Trans. Antennas Propagat.*, vol. 42, pp. 960–966, July 1994.

[33] G. P. Junker, A. A. Kishk, D. Kajfez, A. W. Glisson, and J. Guo, "Input impedance of microstrip-slot-coupled dielectric resonator antennas mounted on thin dielectric layers," *Int. J. Microwave Millimeter-Wave Computer-Aided Eng.*, vol. 6, pp. 174–182, May 1996.

[34] R. F. Harrington, *Time-Harmonic Electromagnetic Fields*. New York: McGraw-Hill, 1961.

[35] J. Van Bladel, *Electromagnetic Fields*. Bristol, PA: Hemisphere, 1985.

[36] L. B. Felsen and N. Marcuvitz, *Radiation and Scattering of Waves*. Englewood Cliffs, NJ: Prentice-Hall, 1973.

[37] J. A. Kong, *Electromagnetic Wave Theory*, 2nd ed. New York: Wiley, 1990.
[38] K. V. Buer and E.-B. El-Sharawy, "A novel technique for tuning dielectric resonators," *IEEE Trans. Microwave Theory Tech.*, vol. 43, pp. 36–41, Jan. 1995.
[39] R. F. Harrington, *Field Computation by Moment Methods*. New York: Macmillan, 1968.
[40] S. V. Yesantharao, "EMPACK—A software toolbox of potential integrals for computational electromagnetics," M.S. thesis, Dept. Elect. Eng., Univ. Houston, Houston, TX, Dec. 1989.
[41] J. Chen, A. A. Kishk, and A. W. Glisson, "A 3D interpolation model for the calculation of the Sommerfeld integrals to analyze dielectric resonator in a multilayered medium," *Electromag.*, vol. 20, no. 1, pp. 1–15, Jan.–Feb. 2000.
[42] D. Kajfez, *Notes on Microwave Circuits*. Oxford, MS: Kajfez Consulting, 1984, vol. 1.
[43] ——, *Q Factor*. Oxford, MS: Vector Fields, 1994.
[44] D. M. Sheen, S. M. Ali, M. D. Abouzahra, and J. A. Kong, "Application of the three-dimensional finite-difference time-domain method to the analysis of planar microstrip circuits," *IEEE Trans. Microwave Theory Tech.*, vol. 38, pp. 849–856, July 1990.
[45] K. A. Michalski and D. Zheng, "Electromagnetic scattering and radiation by surfaces of arbitrary shape in layered media—Part II: Implementation and results for contiguous half-spaces," *IEEE Trans. Antennas Propagat.*, vol. 38, pp. 345–352, Mar. 1990.
[46] G. P. Junker, A. A. Kishk, A. W. Glisson, and D. Kajfez, "Dielectric disk radiating elements," Dept. Elect. Eng., Univ. Mississippi, University, MS, Tech. Rep. 0704-0788, Sept. 1994.
[47] W. Zheng, A. A. Kishk, J. Chen, and C. E. Smith, "Computation of current distribution on cylindrical antennas and scatterers in multi-layer media using a multi-wire model," *Electromag.*, vol. 17, no. 6, pp. 537–562, Nov.–Dec. 1997.
[48] C.-T. Tai, *Dyadic Green's Function in Electromagnetic Theory*. New York: Int. Textbook, 1971.

Jingyang Chen (S'95–M'95) received the B.S. and M.S. degrees from the Beijing Broadcasting Institute, Beijing, China, in 1982 and 1987, respectively, both in electrical engineering, and the M.S. degree in computer science and Ph.D. degree in electrical engineering from the University of Mississippi, University, in 1995 and 1996, respectively.

Since 1996, he has been with the General Instrument Corporation (now the Broadband Communication Sector of Motorola Inc.), San Diego, CA, where he is currently a Technical Staff Member in the Algorithm Group, Uplink Product Department. His current interests include video data compression and video signal processing, especially in noise reduction, rate control, and statistical multiplexing.

Ahmed A. Kishk (S'84–M'86–SM'90–F'98) received the B.S. degree in electrical engineering from Cairo University, Cairo, Egypt, in 1977, the B.S. degree in applied mathematics from Ain-Shams University, Cairo, Egypt, in 1980, and the M.Eng. and Ph.D. degrees from the University of Manitoba, Winnipeg, MB, Canada, in 1983 and 1986, respectively.

He is currently a Professor of electrical engineering at the University of Mississippi, University. His research interest include the areas of design of millimeter frequency feeds for parabolic reflectors, DR antennas, microstrip antennas, corrugated horns, small antenna feeds for parabolic reflectors, mobile satellite antennas, phased-array antennas, and computer-aided design for antennas. He has authored or co-authored over 210 journal and conference papers and technical reports. He is an editor-in-chief of the *ACES Journal*.

Dr. Kishk is a Fellow of IEEE Antennas and Propagation Society (IEEE AP-S) and the IEEE Microwave Theory and Techniques Society (IEEE MTT-S). He is a member of Sigma Xi, Phi Kappa Phi, the U.S. National Committee of International Union of Radio Science (URSI) Commission B, the Applied Computational Electromagnetics Society, and the Electromagnetic Academy. He is an editor for the *IEEE Antennas and Propagation Magazine*. He co-authored *Microwave Horns and Feeds* (London, U.K.: IEE Press, 1994; Piscataway, NJ: IEEE Press, 1994) and *Handbook of Microstrip Antennas* (Stevenage, U.K.: Peregrinus, 1989). He was the recipient of the 1995 Outstanding Paper Award for a paper that appeared in *Applied Computational Electromagnetic Society Journal*. He also received the 1997 Outstanding Engineering Educator Award from Memphis section of the IEEE.

Allen W. Glisson (S'71–M'78–SM'88) received the B.S., M.S., and Ph.D. degrees in electrical engineering from the University of Mississippi, University, in 1973, 1975, and 1978, respectively.

In 1978, he joined the faculty of the University of Mississippi, where he is currently a Professor of electrical engineering. His current research interests include the development and application of numerical techniques for treating electromagnetic radiation and scattering problems, and modeling of DRs and DR antennas. He has been actively involved in the areas of numerical modeling of arbitrarily shaped bodies and bodies of revolution with surface integral-equation formulations. He has served as a consultant to several different industrial organizations in the area of numerical modeling in electromagnetics. He is currently co-editor of the *Applied Computational Electromagnetics Society Journal* and also served as an associate editor for *Radio Science*.

Dr. Glisson is a member of Sigma Xi, Tau Beta Pi, Phi Kappa Phi, and Eta Kappa Nu. He is a member of several professional societies within the IEEE, Commission B of the International Union of Radio Science, and the Applied Computational Electromagnetics Society. He was a U.S. delegate to the 22nd, 23rd, and 24th General Assemblies of URSI. He is currently a member of the IEEE Antennas and Propagation Society (IEEE AP-S) Administrative Committee and the IEEE Press Liaison Committee. Since 1984, he has been the associate editor for book reviews and abstracts for the *IEEE Antennas and Propagation Magazine*. He is currently on the Board of Directors of the Applied Computational Electromagnetics Society. He has also served as secretary of Commission B of the U.S. National Committee of URSI. He was the recipient of a Best Paper Award presented by the SUMMA Foundation and twice received a citation for excellence in refereeing from the American Geophysical Union. He was selected as the University of Mississippi Outstanding Engineering Faculty Member in 1986 and 1996. He was also the recipient of a Ralph R. Teetor Educational Award in 1989.